

UNIVERSITI MALAYSIA PAHANG

DECLARATION OF THESIS AND COPYRIGHT

Author's Full Name : FARIS IMADI BIN AHMAD NADZRI
Identification Card No : 910604-03-5101
Title : DESIGN AND DEVELOPMENT OF
SEDIMENTATION MEASUREMENT DEVICE
FOR MAGNETORHEOLOGICAL FLUID
Academic Session : 2015/2016

I declare that this thesis is classified as:

CONFIDENTIAL

(Contains confidential information under the
Official Secret Act 1972)

RESTRICTED

(Contains restricted information as specified by
the organization where research was done)*

OPEN ACCESS

I agree that my thesis to be published as online
open access (Full text)

I acknowledge that Universiti Malaysia Pahang reserve the right as follows:

1. The Thesis is the Property of University Malaysia Pahang.
2. The Library of University Malaysia Pahang has the right to make copies for the purpose of research only.
3. The Library has the right to make copies of the thesis for academic exchange.

Certified by:

(Author's Signature)

FARIS IMADI BIN AHMAD NADZRI

Date: 21 JUNE 2016

(Supervisor's Signature)

DR IZWAN BIN ISMAIL

Date: 21 JUNE 2016

**DESIGN AND DEVELOPMENT OF SEDIMENTATION
MEASUREMENT DEVICE FOR
MAGNETORHEOLOGICAL
FLUID**

FARIS IMADI BIN AHMAD NADZRI

Report submitted in partial fulfillment of the requirements
for the award of the degree of
Bachelor of Engineering in Manufacturing Engineering

Faculty of Manufacturing Engineering

UNIVERSITI MALAYSIA PAHANG

June 2016

SUPERVISOR'S DECLARATION

I hereby declare that I have checked this thesis and in my opinion, this thesis is adequate in terms of scope and quality for the award of the degree of Bachelor of Engineering in Mechatronics.

Signature :
Name of supervisor : DR IZWAN BIN ISMAIL
Position : SENIOR LECTURER
Date :

STUDENT'S DECLARATION

I hereby declare that the work in this thesis is my own except for quotation and summaries which have been duly acknowledged. The thesis has not been accepted for any degree and is not concurrently submitted for award of other degree.

Signature :

Name : FARIS IMADI BIN AHMAD NADZRI

ID Number : FB12068

Date :

ACKNOWLEDGEMENTS

I am grateful and would like to express my sincere gratitude to my supervisor Doctor Izwan for his germinal ideas, invaluable guidance, continuous encouragement and constant support in making this research possible. He has always impressed me with his outstanding professional conduct, his strong conviction for science, and his belief that a degree program is only a start of a life-long learning experience. I appreciate his consistent support from the first day I applied to graduate program to these concluding moments. I am truly grateful for his progressive vision about my training in science, his tolerance of my naïve mistakes, and his commitment to my future career. I also sincerely thank for the time spent proofreading and correcting my many mistakes.

My sincere thanks go to all my lab mates and members of the staff of the Machining Lab and Material Lab, UMP, who helped me in many ways and made my stay at UMP pleasant and unforgettable.

I acknowledge my sincere indebtedness and gratitude to my parents for their love, dream and sacrifice throughout my life. Special thanks should be given to my committee members. I would like to acknowledge their comments and suggestions, which was crucial for the successful completion of this study.

ABSTRACT

The measurement of particles sedimentation in the magnetorheological fluid (MRF) can be performed by the method of visual inspection, digital photography and electromagnetic induction. However, the visual inspection method produces poor accuracy result due to the observer's parallax error. While the digital photography method requires proper lighting in order to obtain good image before it can be processed. For electromagnetic induction method, the sedimentation measurement only can be performed to particles that have good magnetic permeability. To overcome these drawbacks, laser light transmission may become the alternative method for measuring the particle sedimentation. This thesis discusses about design and development of a sedimentation measurement device for MRF based on laser light transmission. The objectives of the work are to design and fabricate a prototype of settling monitoring device based on light transmission by using a laser diode as light source and a photodiode as photodetector, to verify the reliability of the light transmission-receiving system of the prototype by using ultraviolet–visible (UV-Vis) spectrophotometer, and to evaluate the prototype by measuring the sedimentation rate of iron particles in three MRF types with different composition. The sedimentation measurement device was designed and developed. For the light transmission-receiving system, a laser diode (650 nm) was used as light transmitter and a photodiode was used as light receiver. The reliability of this system was evaluated by locating the wavelength that give the highest particles detection at clear part of three different MRF samples. The result for this experiment suggest that the wavelength ranging from 411 nm to 421 nm give the highest level of the particles detection. Besides that, the comparison between the light absorbance of the clear parts of the three samples measured by UV-Vis spectrophotometer and measured by the developed device was carried out. The outcome from the comparison shows that the light detector used in the prototype could not give the same detection sensitivity as the light detector of the UV-Vis spectrophotometer due to the mismatch between the laser wavelength and the photodiode peak sensitivity wavelength. In addition, the developed device also was evaluated by conducting the sedimentation analysis for three different compositions of MRF samples. The evaluation result presents that the prototype was able to perform the sedimentation monitoring for the samples examined.

ABSTRAK

Pengukuran pemendapan zarah dalam cecair *magnetorheological* (MRF) boleh dilakukan dengan kaedah pemeriksaan visual, fotografi digital dan aruhan elektromagnet. Walau bagaimanapun, kaedah pemeriksaan visual menghasilkan keputusan yang tidak tepat kerana ralat paralaks pemerhati. Manakala kaedah fotografi digital memerlukan pencahayaan yang betul untuk mendapatkan imej yang baik sebelum ia boleh diproses. Untuk kaedah aruhan elektromagnet pula, pengukuran pemendapan hanya boleh dilakukan kepada zarah yang mempunyai kebolehtelapan magnet yang baik. Untuk mengatasi kelemahan ini, penghantaran cahaya laser boleh menjadi kaedah alternatif untuk mengukur pemendapan zarah tersebut. Tesis ini membincangkan tentang reka bentuk dan pembangunan peranti pengukuran pemendapan untuk MRF berdasarkan penghantaran cahaya laser. Objektif kerja ini adalah untuk mereka bentuk dan membina sebuah peranti pengawasan pemendapan berdasarkan penghantaran cahaya dengan menggunakan diod laser sebagai sumber cahaya dan fotodiod sebagai pengesan foto, untuk mengesahkan kebolehpercayaan sistem penghantaran-menerima cahaya prototaip dengan menggunakan ultraviolet boleh dilihat (UV-Vis) spektrofotometer, dan untuk menilai prototaip dengan mengukur kadar pemendapan zarah besi dalam tiga jenis MRF dengan komposisi yang berbeza. Peranti pengukuran pemendapan telah direka dan dibangunkan. Untuk sistem penghantaran-penerimaan cahaya, diod laser (650 nm) digunakan sebagai pemancar cahaya dan fotodiod digunakan sebagai penerima cahaya. Kebolehpercayaan sistem ini dinilai dengan mencari panjang gelombang yang memberi tahap pengesanan zarah yang paling tinggi dalam bahagian jernih bagi tiga sampel MRF yang berlainan. Keputusan bagi eksperimen ini menunjukkan bahawa panjang gelombang antara 411 nm hingga 421 nm memberi tahap pengesanan zarah dalam bahagian jernih sampel MRF yang paling tinggi. Selain itu, perbandingan di antara kuantiti serapan cahaya oleh bahagian jernih sampel yang diukur dengan spektrofotometer UV-Vis dan yang diukur oleh peranti telah dijalankan. Hasil daripada perbandingan menunjukkan bahawa pengesan cahaya digunakan dalam prototaip tidak dapat memberikan sensitiviti pengesanan yang sama seperti pengesan cahaya bagi spektrofotometer UV-Vis kerana ketidaksinambungan antara panjang gelombang laser dan puncak sensitiviti gelombang bagi fotodiod. Di samping itu, peranti ini juga telah dinilai dengan menjalankan analisis pemendapan terhadap tiga sampel MRF dengan komposisi yang berbeza. Hasil penilaian membentangkan bahawa prototaip dapat melakukan pemantauan pemendapan bagi sampel-sampel yang diperiksa.

TABLES OF CONTENT

| | Page |
|---|-------------|
| SUPERVISOR’S DECLARATION | iii |
| STUDENT’S DECLARATION | iv |
| ACKNOWLEDGEMENTS | v |
| ABSTRACT | vi |
| ABSTRAK | vii |
| TABLE OF CONTENTS | viii |
| LIST OF TABLES | x |
| LIST OF FIGURES | xi |
| LIST OF SYMBOLS | xiii |
| LIST OF ABBREVIATIONS | xvi |
| CHAPTER 1 INTRODUCTION | |
| 1.1 Project Background | 1 |
| 1.2 Problem Statement | 2 |
| 1.3 Objectives | 2 |
| 1.4 Scope of Work | 2 |
| 1.5 Expected Outcome | 3 |
| CHAPTER 2 LITERATURE REVIEW | |
| 2.1 Colloidal Dispersion | 4 |
| 2.1.1 Sedimentation | 5 |
| 2.1.2 Technique of Sedimentation Analysis | 5 |
| 2.2 Magnetorheological Fluids | 8 |
| 2.2.1 MRF Characteristic | 9 |
| 2.2.2 Stability in MRF | 10 |
| 2.3 Light Scattering | 10 |
| 2.3.1 Static Light Scattering | 10 |
| 2.3.2 The Rayleigh Ratio | 11 |

| | | |
|-------|-------------------------------|----|
| 2.3.3 | Light as Electromagnetic Wave | 12 |
| 2.3.4 | Electric Dipole | 14 |
| 2.4 | Lasers | 15 |
| 2.4.1 | Laser Diode | 15 |
| 2.4.2 | Laser Diode Property | 16 |
| 2.5 | Photodiode | 17 |
| 2.5.1 | Photodiode Circuits | 19 |

CHAPTER 3 METHODOLOGY

| | | |
|-------|--|----|
| 3.1 | Design and Fabrication Process | 21 |
| 3.1.1 | Design Concept | 22 |
| 3.1.2 | Prototype Design and Fabrication | 24 |
| 3.2 | Experimental Works | 30 |
| 3.2.1 | Verification Experiment Using UV-Vis Spectrophotometer | 30 |
| 3.2.2 | Sedimentation Experiment Using the Developed Prototype | 34 |

CHAPTER 4 RESULTS AND DISCUSSION

| | | |
|-----|--|----|
| 4.1 | Fabricated Prototype of Settling Monitoring Device | 36 |
| 4.2 | Verification Experiment Results and Discussion | 38 |
| 4.3 | Sedimentation Experiment | 41 |

CHAPTER 5 CONCLUSION AND RECOMMENDATIONS

| | | |
|-----|----------------|----|
| 5.1 | Conclusion | 46 |
| 5.2 | Recommendation | 47 |

| | |
|-------------------|----|
| REFERENCES | 49 |
|-------------------|----|

| | |
|-------------------|----|
| APPENDICES | 51 |
|-------------------|----|

| | |
|---|----|
| A | 51 |
|---|----|

LIST OF TABLES

| Table No. | Title | Page |
|------------------|---|-------------|
| 2.1 | Colloidal dispersion types with examples (Dobias et al., 1999) | 4 |
| 3.1 | Sample with different component composition and their volume percentage | 31 |
| 4.1 | Absorbance comparison between UV-Vis spectrophotometer and prototype | 41 |

LIST OF FIGURES

| Figure No. | Title | Page |
|-------------------|--|-------------|
| 2.1 | An experiment setup of visual inspection method | 5 |
| 2.2 | Schematic image of the stability determination system (Rabbani, Ashtiani, & Hashemabadi, 2015) | 7 |
| 2.3 | An experiment setup of electromagnetic induction method (López-López, Zugaldía, González-Caballero, & Durán, 2006) | 8 |
| 2.4 | The state which no external magnetic field applied to MRF (Kciuk & Turczyn, 2006) | 9 |
| 2.5 | The state when the external magnetic field is applied to MRF (Kciuk & Turczyn, 2006) | 9 |
| 2.6 | An illustration of light scattering experiment setup | 11 |
| 2.7 | Propagation of electromagnetic wave (Ogendal, 2013) | 13 |
| 2.8 | An illustration of the electric dipole for a pair of opposite charges (a) An electric dipole. (b) A particle become a dipole when subjecting to external electric field. | 14 |
| 2.9 | A laser diode made by Opnext-Hitachi (Kasap, 2013) | 15 |
| 2.10 | Input-output relationship of typical laser diode | 16 |
| 2.11 | Beam divergence of laser diode (Quimby, 2006) | 17 |
| 2.12 | Various sizes of Si photodiode (Kasap, 2013) | 18 |
| 2.13 | Basic operation of photodiode (a) Photodiode in reverse biased (b) I–V characteristics of the photodiode (c) current–voltage converter or a transimpedance amplifier | 19 |
| 3.1 | Flowchart of research methodology | 21 |
| 3.2 | Prototype sketching | 23 |
| 3.3 | An illustration of prototype three dimensional sketching | 24 |
| 3.4 | Detail prototype design | 25 |
| 3.5 | An exploded view of prototype design | 26 |

| | | |
|------|--|----|
| 3.6 | Light transmission-receiving system for the prototype (a) sensor circuit, (b) laser diode circuit | 27 |
| 3.7 | Arduino programming for interfacing with photodiode circuit | 28 |
| 3.8 | CoolTerm application captured the sensor data and saved it in asc. file | 29 |
| 3.9 | Three different MRF samples | 31 |
| 3.10 | An UV-Vis spectrophotometer model GENESYS™ 10S | 32 |
| 3.11 | An illustration of three different parts that existed after particle sedimentation | 33 |
| 3.12 | 1 cm × 1 cm plastic cuvette that was used to hold the samples' clear part in order to examine using UV-Vis spectrophotometer | 34 |
| 3.13 | Sedimentation rate of a sample is being tested | 35 |
| 4.1 | A photo of completed prototype | 37 |
| 4.2 | A photo of completed circuits | 37 |
| 4.3 | Absorbance reading by UV-Vis spectrophotometer with variation of wavelengths (390 nm-780 nm) | 39 |
| 4.4 | An illustration of light absorption process of a matter | 40 |
| 4.5 | Sedimentation ratio measurement by using developed prototype | 42 |
| 4.6 | The magnified view of sedimentation plot for sample 1 | 43 |
| 4.7 | The magnified view of sedimentation plot for sample 2 | 44 |
| 4.8 | The magnified view of sedimentation plot for sample 3 | 44 |
| 4.9 | A photo of sample 2 (a) Initial experiment, (b) minute of 395, (c) minute of 428 and (d) final experiment | 45 |

LIST OF SYMBOLS

| | |
|---------------|---|
| S_R | Sedimentation ratio |
| H_S | Height of supernatant fluid |
| H_T | Total height of sample fluid |
| V_C | Volume of clear liquid |
| V_T | Volume of total suspension |
| R_θ | Rayleigh ratio |
| $I_S(\theta)$ | Scattered light intensity |
| I_O | Intensity of the laser |
| $V_S(\theta)$ | Scattering volume brightened by laser |
| r | Distance from scattering volume to detector |
| θ | Scattering angle |
| \vec{q} | Scattering vector |
| q | Scattering length |
| n | Refractive index of medium |
| \vec{E} | Electric field |
| E_o | Amplitude of the electric field component of light |
| \vec{B} | Magnetic field |
| λ | Light wavelength |
| λ_o | Wavelength of the light in vacuum |
| f | Light frequency |
| c | Speed of light |
| h | Plank constant |
| ϕ | Phase of cosine function at time $t = 0$ and at $x = 0$ |

| | |
|--------------|---------------------------|
| t | Time |
| x | Wave propagation distance |
| k | Wavenumber |
| \vec{k} | Wavevector |
| $ \vec{k} $ | Vector length |
| \vec{r} | X -coordinate vector |
| ϵ_0 | Vacuum permittivity |
| μ | Dipole moment |
| Q | Charge magnitude |
| $+Q$ | Positive-charge |
| $-Q$ | Negative-charge |
| R_F | Feedback resistor |
| C | Capacitor |
| V_{out} | Output voltage |
| V_f | Final voltage |
| V_i | Initial voltage |
| V | Voltage |
| V | Volt |
| I | Current |
| I_{in} | Input current |
| I_{TH} | Threshold current |
| I_{ph} | Photocurrent |
| I_{sc} | Short circuit current |
| A | Ampere |

| | |
|----------------------------|---|
| P_{out} | Output power |
| P_o | Incident light power |
| P | Radiant power emitted by light source |
| P_L | Radiant power leaving the sample |
| d | Active region thickness |
| $\Delta\theta_{\perp}$ | Half-width perpendicular to layer |
| w | Width of the active region parallel to the junction |
| $\Delta\theta_{\parallel}$ | Half-width parallel to layer |
| R | Responsivity |
| R | Resistance |
| R_L | Load resistance |
| Vr | Reverse voltage |
| P | Operating point |
| T | Transmittance |
| A | Absorbance |
| E | Energy |
| E_{photon} | Photon energy |
| ΔE | Energy different |
| Cu | Copper |
| SiO_2 | Silicon dioxide |

LIST OF ABBREVIATIONS

| | |
|--------|--|
| CIP | Carbonyl iron powder |
| CIMs | Carbonyl iron microparticles |
| CATIA | Computer aided three-dimensional interactive application |
| DC | Direct current |
| ERF | Electrorheological fluid |
| FWHM | Full width at half maximum |
| HO | Hydraulic oil |
| MRF | Magnetorheological fluid |
| OPAMP | Operational amplifier |
| PVC | Polyvinyl chloride |
| SLS | Static light scattering |
| UV-Vis | Ultraviolet–visible |

CHAPTER 1

INTRODUCTION

1.1 PROJECT BACKGROUND

Sedimentation is a natural phenomenon that can be found happen in dispersed system such as colloidal suspension. This phenomenon become a shortcoming to materials like electrorheological fluid (Hazzab, Terfous, & Ghenaim), nanofluid and magnetorheological fluid (MRF). Prekas (2013) stated in his research that the long-term sedimentation can affect the electrorheological phenomenon and the exploitable electromechanical and viscoelastic properties regardless of the existence of the stimulating electric field (Prekas et al., 2013). While Murshed (2008) found that this drawbacks that also possess by nanofluids can make the heat transfer devices clogging in its walls (Murshed, Leong, & Yang, 2008). Besides that, smart material such magneto rheological fluids suffer the lacking of performance because of this kind of defect (Xu, Guo, & Chen, 2014). Because of these problem, stability analysis become a great concern among scientists and engineers in developing those materials.

Sedimentation measurement can be done by naked eyes so-called visual inspection. For convenience and accuracy, various method has been developed for analysing sedimentation behaviour of dispersions. Rabbani (2015) successfully used digital photography method in his investigation of stability properties of a suspension of carbonyl iron microparticles (CIMs) in silicone oil (Rabbani et al., 2015). While López-López (2006) analysed the sedimentation behaviour of iron-based magnetorheological fluids by using an electromagnetic induction method (López-López et al., 2006). Hazzab

(2008) used video camera to monitor the settling velocity of polyvinyl chloride (PVC) in fluids (Hazzab, Terfous, & Ghenaim, 2008). However, these methods have their own disadvantages in determining sedimentation measurement.

1.2 PROBLEM STATEMENT

Solid particles that dispersed in fluid may completely settle for a period of more than 24 hours. This period of time is too long for researchers to monitor the sedimentation without the help of machines. As a human, visual inspection by naked eye to monitor the sedimentation behaviour will produce less accurate result due to the parallax error. This error can be overcome by the use of digital photography method to monitor this event. Nevertheless, this method needs proper lighting in order to obtain good image before it can be processed (Petschnigg et al., 2004). Other method that can substitute digital photography is by the use of electromagnetic induction method. But this technique only can be applied to particles that have good magnetic permeability. Light transmission may become the alternative method to be used for sedimentation analysis to avoid these problems.

1.3 OBJECTIVES

- i. To design and fabricate a prototype of settling monitoring device based on light transmission by using a laser diode as light source and a photodiode as photodetector.
- ii. To verify the reliability of the light transmission-receiving system of the prototype by using ultraviolet–visible (UV-Vis) spectrophotometer.
- iii. To evaluate the prototype by measuring the sedimentation rate of iron particles in three MRF types with different compositions.

1.4 SCOPE OF WORK

The light source used is 5mW red laser diode with the wavelength of 650 nm. As a light receiver, a silicon photodiode with the range of spectral bandwidth of 420 nm to 675 nm was used. Transimpedance amplifier was developed to operate the photodiode.

The sedimentation rate of MRF was determined by measuring the voltage output from the sensor that generated by the light power received from the laser diode after passing through the samples.

The development work of this instrument was only focus on sedimentation behaviour in MRF. The sedimentation for three MRF samples with different composition were evaluated by the prototype. The components used in the MRF samples include carbonyl iron powder (CIP), hydraulic oil (HO), copper (Cu) and silicon dioxide (SiO₂). Sample 1 is composed of CIP, HO, and SiO₂, sample 2 is composed of CIP, HO, Cu and SiO₂, while sample 3 is composed of CIP, HO and Cu

The reliability of the light transmission-receiving system was verified by performing two experiments. The first experiment is locating the wavelength that give the maximum absorbance reading measured at the clear part of MRF samples. Whilst, the second experiment is making comparison between the light absorbance of the samples' clear part measured by the developed device and measured by UV-Vis spectrophotometer.

1.5 EXPECTED OUTCOME

- i. An instrument that can reliably measure the sedimentation rate of MRF with different components.
- ii. The device is expected to possess the ability to monitor and record the sedimentation measurement result in real time.

CHAPTER 2

LITERATURE REVIEW

2.1 COLLOIDAL DISPERSION

Colloidal dispersion is a kind of heterogeneous mixture that composed of at least two different phase that is disperse phase and dispersion medium. The state of matter for both disperse phase and dispersion medium can be solid, liquid, or gas state. Various products such as paints, pharmaceuticals, cosmetics, are made up based on colloidal system. Colloidal dispersion can be classified based on the state of aggregation of the dispersed phase and the dispersion medium (Dobias, Qiu, & von Rybinski, 1999). Table 2.1 shows the possible combinations of dispersed phase and dispersion media along with the examples of exist product.

Table 2.1: Colloidal dispersion types with examples

| Dispersed phase | Dispersion medium | Technical name | Examples |
|------------------------|--------------------------|-----------------------|------------------------|
| Solid | Solid | Solid dispersion | Ruby glass |
| Liquid | Solid | Solid emulsion | Ice cream |
| Gas | Solid | Solid foam | Insulating foam |
| Solid | Liquid | Sol or dispersion | Paint, printing ink |
| Liquid | Liquid | Emulsion | Milk, rubber |
| Gas | Liquid | Foam | Fire extinguisher foam |
| Solid | Gas | Aerosol | Smoke |
| Liquid | Gas | Aerosol | Hairspray, dust, fog |

Source: Dobias et al (1999)

2.1.1 Sedimentation

Sedimentation is the inclination of the particles in suspension to simmer down in the fluid in which they are entrapped and come to rest in opposition to a resistance. This happen because of their movement through the fluid in reaction to the forces imposing on them. Gravity, centrifugal acceleration or electromagnetism become the cause of that force (Kumar & Mangal, 2013). Particle characteristics are used to ascertain the sedimentation behaviour. That characteristics are size, particle–particle interaction, density of particles which mainly depends on granular, physicochemical or hydrodynamic conditions, or weight concentration (Azema, 2006).

2.1.2 Technique of Sedimentation Analysis

Sedimentation analysis for suspensions can be done by the method of visual inspection. Figure 2.1 illustrate the experiment setup of visual inspection method.

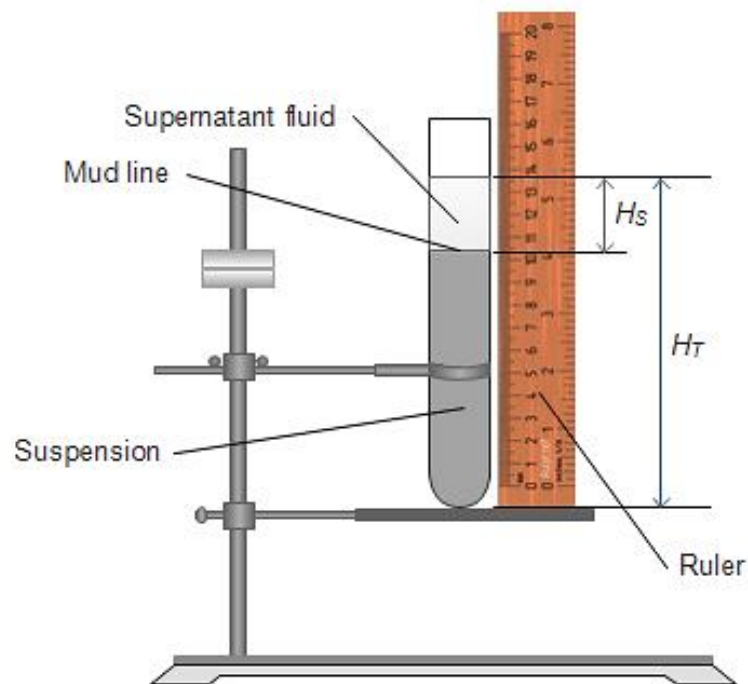


Figure 2.1: An experiment setup of visual inspection method

This set up contains a tube holding device and a ruler which is placed adjacent to the test tube to measure the height of supernatant fluid. With passage of time, the height of supernatant fluid increases and the height of turbid part decreases. The sedimentation is observed visually at day time to get a clear view of the observation being made for the height of supernatant and the turbid part of the suspension. The suspension is left in cylindrical glass test tube for certain time at vertical stationary position. The height of the supernatant fluid is measured after every certain interval with the help of ruler and stop watch. Thus, sedimentation ratio is calculated. The sedimentation ratio is defined as the ratio of the height of the supernatant oil to the total height of the suspension filled and is given as

$$S_R = \frac{H_S}{H_T} \times 100\% \quad (2.1)$$

where S_R is the sedimentation ratio, H_S is the height of supernatant fluid and H_T is the total height of sample fluid filled in the tube (Kumar & Mangal, 2013).

To get more precise result, vision monitoring technique that consist of a camera, a computer with image processing application, chronometer and lighting can be used. In this method, suspensions are kept in a fixed place for some passage of time and photographed within certain time intervals. Afterwards, the height and volume of each phase were determined through image processing, which represented a bi-phased suspension (Rabbani et al., 2015). Figure 2.2 shows the schematic image of the stability determination system. The sedimentation ratio S_R is defined as the ratio of the clear liquid volume V_C to the total suspension volume V_T as follows

$$S_R = \frac{V_C}{V_T} \times 100\% \quad (2.2)$$

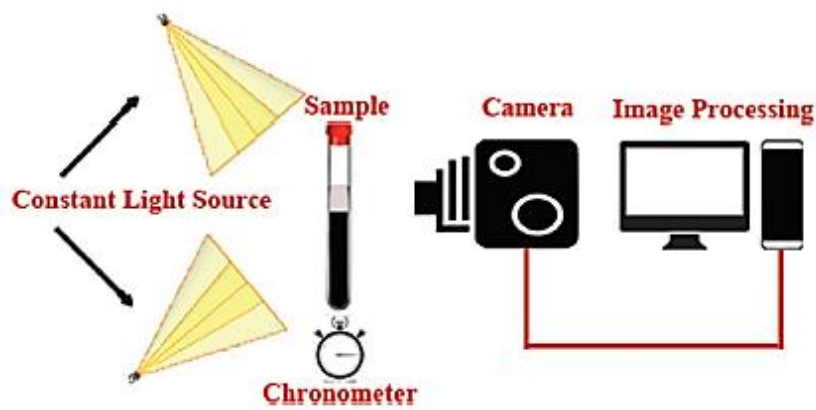


Figure 2.2: Schematic image of the stability determination system

Source: (Rabbani et al., 2015)

Other analysis technique that can be implemented is electromagnetic induction method. This method is based on the time evolution of the electromotive force induced in a coil that surrounds the sample. This method only possible for particles with good permeability. By referring Figure 2.3, the experimental setup consists of a pair of Helmholtz coils, which are used for producing an alternating magnetic field of low intensity in the vertical direction. A cylindrical test tube containing a magnetic suspension is placed in the centre of the Helmholtz coils along their axial direction, and a small sensing coil is placed around the test tube. During the sedimentation experiments, the value of the induced potential in the sensing coil, V , was measured as a function of time (López-López et al., 2006).

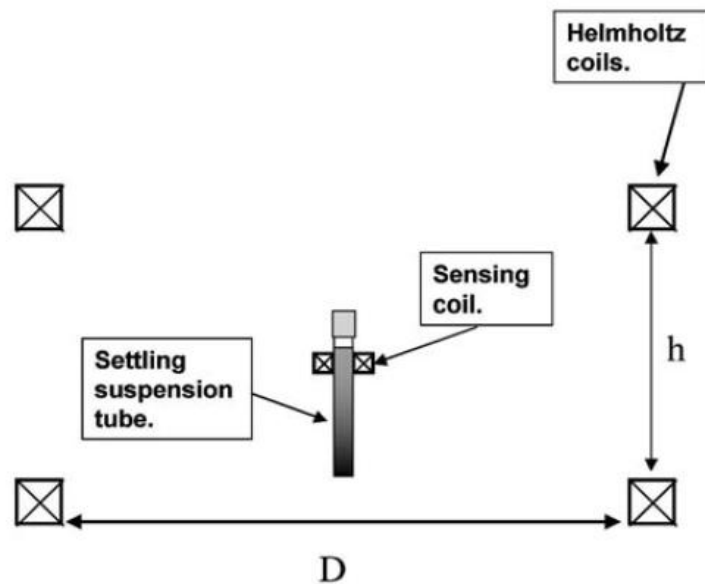


Figure 2.3: An experiment setup of electromagnetic induction method

Source: (López-López et al., 2006)

2.2 MAGNETORHEOLOGICAL FLUIDS

Magnetorheological Fluids (MRF) are categorized as smart material that when applying a magnetic field to it, their rheological properties become quickly changed. These materials primarily contain magnetic particles (mainly iron), carrier fluid and additives. The carrier fluid will act as low permeability and non-magnetic base liquid that in which the magnetically active phase particles remain suspended. After hydrocarbon oil, the most frequently used carrier liquid is silicon oil (Kumar & Mangal, 2013). Fluid such paraffin oil, mineral oil and hydraulic oil also can be used as carrier fluid.

The purposes of using additives in MRF are to prevent and minimize sedimentation, to prevent and minimize coagulating of the particles, to preserve a coating on the particles in order to intensify re-dispersibility and to increase anti-oxidation. When silicone oil is used base liquid, additive such white lithium grease is a good match with this carrier fluid (Kumar & Mangal, 2013). Other additives role is as surfactants which is used to increase the polarization induced in the suspended particles when a magnetic field is imposed (Kciuk & Turczyn, 2006).

2.2.1 MRF Characteristic

Typically, the diameter of the magnetisable particles ranges from 3 to 5 microns. Smaller particles size makes MRF more stable but it is difficult to manufacture such particles. By having a diameter of 30 nanometres, MRF which is created from pigment that usually found in magnetic recording media particles are quite stable. MRF can be estimated as Newtonian liquids when there is no external magnetic field applied to it. In the presence of an applied magnetic field, the iron particles will form linear chains aligned to the magnetic field (Kciuk & Turczyn, 2006). Figure 2.4 and Figure 2.5 illustrate the two state of MRF.

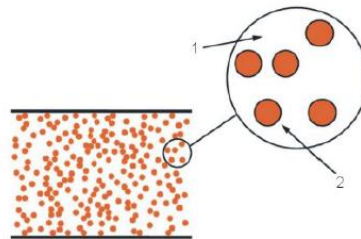


Figure 2.4: The state which no external magnetic field applied to MRF

Source: (Kciuk & Turczyn, 2006)

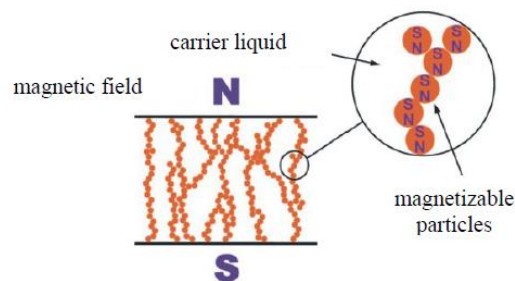


Figure 2.5: The state when the external magnetic field is applied to MRF

Source: (Kciuk & Turczyn, 2006)

2.2.2 Stability in MRF

Suspension stability or sedimentation stability become one of the significant factor that affect the performance of MRF. In the absence of external magnetic field, the settlement happens due to the action of gravity field. Great different density between the magnetic particles and carrier fluid makes the settlement takes place more easily though experiencing some fluid resistance. Other factor that contribute to particles settlement in fluid are the effect of Brownian motion. The size and temperature of particle determine the state of this motion (Zhou Feng*, 2015).

2.3 LIGHT SCATTERING

Light scattering is a phenomenon that happen when light strikes a particle or a cluster of particles then cause its direction of propagation change. Scattering can be categorised to two type that is elastic and inelastic. Light scattering is said elastic when the wavelength of scattered light precisely the same wavelength as the incident light. While light scattering is said inelastic if there is a change of the scattered light wavelength relative to the incident light. Raman scattering and Brillouin scattering are some examples of inelastic light scattering. Quasi light scattering is an example of elastic scattering (Ogental, 2013).

2.3.1 Static Light Scattering

Static light scattering (SLS) is a technique that use to measure the size of particles and the molecular weight of macromolecules. This technique is based on the nature of light that as light passes through a solution contained particles some portion of the light will be scattered in all directions. The solution of particles that illuminated by light appears completely opaque when all light is scattered. In other situation the solution looks completely transparent if the scattered portion of light is too small.

Light sources to be used in SLS must possess a well-defined wavelength (monochromatic) and its rays have to be parallel (collimated beam) (Ogental, 2013). Non-monochromatic such common white light composed of all wavelengths between roughly 390 and 700 nm is not suitable to use for this method. Lasers are convenient light

source to use because it is monochromatic and have collimated beam. Other advantage from utilising lasers is its beam can be polarised according to desired direction.

2.3.2 The Rayleigh Ratio

The Rayleigh ratio, R is a parameter used in light scattering experiment on a suspension. This parameter is used so that the deduced properties of that suspension is independent of apparatus characteristics. Rayleigh ratio of a solution under investigation can be define as

$$R_{\theta} = \frac{I_S(\theta).r^2}{I_0.V_S(\theta)} \quad (2.3)$$

where the subscript R_{θ} is the Rayleigh ratio with a function of the scattering angle, $I_S(\theta)$ is the intensity of the scattered light measured at the angle of detector (refer Figure 2.6), I_0 is the intensity of the laser used, $V_S(\theta)$ is the scattering volume which is brightened by the laser while at the same time being visible for the detector (refer Figure 2.6), and r is the distance from the scattering volume to the detector.

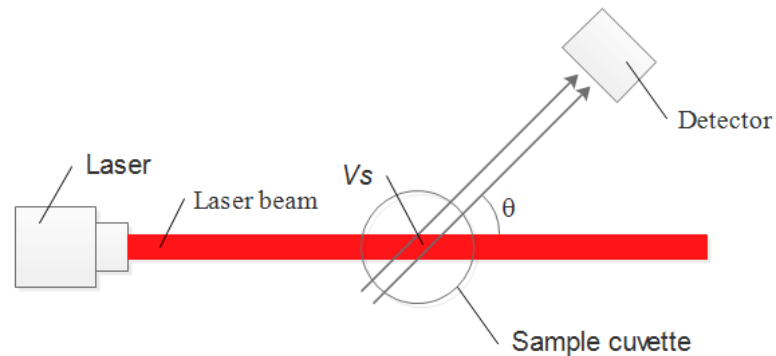


Figure 2.6: An illustration of light scattering experiment setup

To makes the equations defining light scattering become easier, the scattering angle θ can be replaced scattering vector \vec{q} where the length of q can be calculated as $q = (4\pi n/\lambda)\sin(\theta/2)$ where n is the medium refractive index and λ is the wavelength of the light in the medium through which the light propagates. Then the Rayleigh ratio become

$$R_q = \frac{I_S(q) \cdot r^2}{I_0 \cdot V_S(q)} \quad (2.4)$$

2.3.3 Light as Electromagnetic Wave

Light can be described whether as particles so-called photons or as electromagnetic waves (Serway & Jewett, 2013). In the case of light scattering, it is appropriate to treat light as electromagnetic waves. As the name implies, electromagnetic waves are resulting from the combination of electric wave and magnetic wave. They mutually generating each other when they propagate with the same speed as light. Figure 2.7 illustrate how an electromagnetic wave propagates along an axis. The electric field \vec{E} and the magnetic field \vec{B} are perpendicular to each other and to the direction of propagation.

Light is said to be vertically polarised if the electric field oscillating in the direction of the z-axis while it propagates along the x-axis. If the vertically polarised light is of one wavelength λ its electric field can be described by

$$E(x, t) = E_z(x, t) = E_o \cos\left(2\pi f \left(t - \frac{x}{c}\right) + \phi\right) \quad (2.5)$$

where f is the frequency of the light, c is the speed of light and E_o is the amplitude of the electric field component of the light. The subscript ϕ define the phase of the cosine function at time $t = 0$ and at $x = 0$. In light scattering, magnetic field usually can be ignored as it normally does not interact with organic matter.

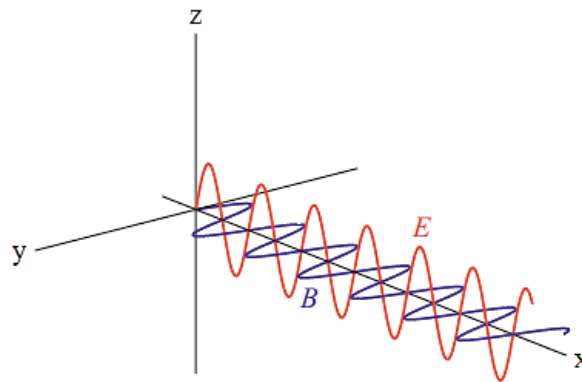


Figure 2.7: Propagation of electromagnetic wave

Source: (Ogendal, 2013)

Equation 2.5 can be simplified by defining the wavenumber k as $k = 2\pi n/\lambda_o$ where λ_o is the wavelength of the light in vacuum and n is the refractive index of the medium. Besides that, term $2\pi f$ can be replaced with ω and as $f/c = 1/\lambda$ equation 2.5 can be written as

$$E(x, t) = E_y(x, t) = E_o \cos(\omega t - kx + \phi) \quad (2.6)$$

The equation 2.6 can be generalised to propagation in any direction by substituting the wavenumber k to wavevector \vec{k} defined as a vector pointing in the direction of propagation and with a length $|\vec{k}| = 2\pi n/\lambda_o$. The x -coordinate is substituted by a Then equation 2.6 becomes

$$E(\vec{r}, t) = E_o \cos(\omega t - k\vec{r} + \phi) \quad (2.7)$$

By referring to electromagnetic wave the intensity of the light is given by the time average of the square of the electric field:

$$I_o(x) = \epsilon_o c \langle E^2(x, t) \rangle \quad (2.9)$$

Where $\epsilon_o = 8.85 \times 10^{-12} \text{F.m}^{-1}$ is the vacuum permittivity and $c = 3 \times 10^{-1} \text{m.s}^{-1}$ is the speed of light in vacuum. Substituting equation 2.7 into equation 2.9 yield

$$I_o(x) = \epsilon_o c E_o^2 \langle \cos^2(\omega t - \vec{k} \cdot \vec{r}) \rangle \quad (2.10)$$

As the mean value of $\cos^2(\omega t - \vec{k} \cdot \vec{r})$ calculated over even extremely short time intervals is $\frac{1}{2}$, then the resulting of equation 2.10 is

$$I_o(x) = \frac{1}{2} \epsilon_o c E_o^2 \quad (2.11)$$

2.3.4 Electric Dipole

An electric dipole is an object which has an asymmetrical distribution of charge. Usually that object has one end with positive charge and the other end with negative charge (Ogendal, 2013). Figure 2.8 show an electric dipole and the multiplication of the charge magnitude Q to the distance between the positive-charge $+Q$ and the negative-charge $-Q$ is define as dipole moment μ as shown in Figure 2.8 a). There are two type of dipole moment that is permanent and induced. Only induced dipole momenta that have relation to light scattering.

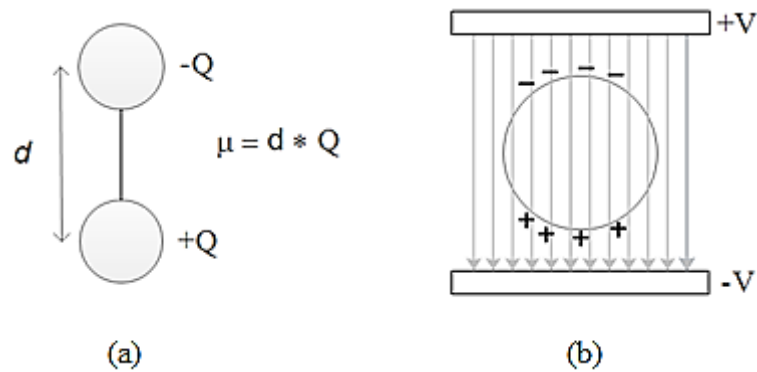


Figure 2.8: An illustration of the electric dipole for a pair of opposite charges (a) An electric dipole. (b) A particle become a dipole when subjecting to external electric field.

2.4 LASERS

Lasers are devices that emit a highly focus light beam with a very authentic wavelength or frequency cause by the amplified light intensity. The generated power range of lasers can be start from Nano watts to a billion trillion watts. The range of the produced wavelengths or frequencies is start from microwave region and infrared to the visible, ultraviolet, vacuum ultraviolet, and to the soft-X-ray spectral regions. Lasers are widely used in modern communication system, industrial and medical worlds. Usually, lasers are built not to produce white light but instead produce a specific colour based on application need (Jenkins & White, 2001).

2.4.1 Laser Diode

A laser diode is a man-made light source that generate light by the process of stimulated emission. In this process, the likelihood that a photon is produced based on the number of photons already exist. With the extra photons being created by the existing photon, the light become amplified. By integrating reflective components to the ends of the semiconductor, this amplification can be created self-sustaining. When multiple passes is made by the light through the device, it is continuously amplified until laser light is generated (Quimby, 2006). Figure 2.9 shows the example of laser diode made by Opnext-Hitachi.



Figure 2.9: A laser diode made by Opnext-Hitachi

Source: (Kasap, 2013)

2.4.2 Laser Diode Property

Input-output relationship of typical laser diode can be illustrated as in Figure 2.10. Based on this figure, the device does not operate as a laser when the input current I_{in} is lower than threshold current I_{TH} because the optical power is low. As the current is beyond the I_{TH} , the output power P_{out} increase linearly with the current increment until it reach a saturated value. In optical communication a diode laser can be characterize by efficiency, beam divergence, spectral purity, threshold current, etc.

Efficiency is a quality that show the laser output power generated for a certain supplied current in a specified time interval. “Quantum efficiency” is also used to qualify this property for the purpose of precise measure. This kind of efficiency can be defined as the number of output photons divided by the number of input electrons. The design of laser diode driver circuit should be based on this property.

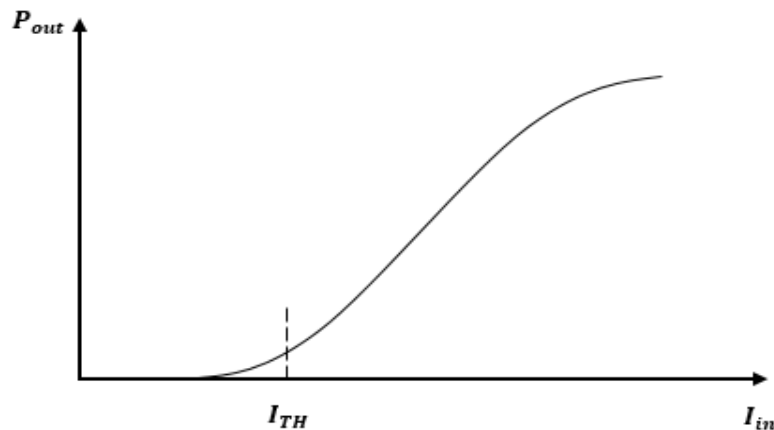


Figure 2.10: Input-output relationship of typical laser diode

Beam divergence of a laser diode is determine based on the angular angle of perpendicular to the plane of the junction and angular angle of parallel to that plane. Usually, this property is well informed by using the term “full width at half maximum (FWHM)” in the laser diode datasheet. By referring Figure 2.11, the angular spread of light is calculated by these two equation

$$\Delta\theta_{\perp} = \frac{\lambda}{d} \quad (2.12)$$

$$\Delta\theta_{\parallel} = \frac{\lambda}{w} \quad (2.13)$$

where λ is wavelength after leaving the diode, d is the active region thickness, $\Delta\theta_{\perp}$ is the half-width perpendicular to layer, w is the width of the active region parallel to the junction and $\Delta\theta_{\parallel}$ is the half-width parallel to layer.

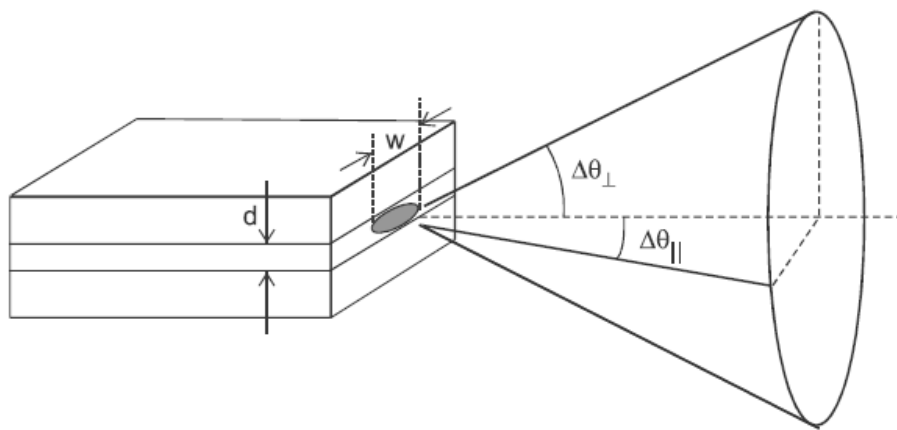


Figure 2.11: Beam divergence of laser diode

Source: (Quimby, 2006)

2.5 Photodiode

Photodiode is a kind of junction diode made of semiconductor material which sensitive to light. In semiconductors, the escaping electrons from the valence band is related to the supplied energy to it. Heat, accelerating voltage, and light energy can be the sources of that energy. The function of photodiode is to absorb light energy and convert it to electrical current. Many types of photodiodes that available in the market commonly made of germanium, silicon, lead sulphide, indium gallium arsenide and many more (Mallik, 2013). The operation of photodiode is based on two type of bias mode namely forward bias and reverse bias which determine the flows of photo current in it. Figure 2.12 illustrates various sizes of Si photodiode made by Hamamatsu.

There are variety of photodiode technology with different properties has been developed to suite application needs. PN photodiode is the initial photodiode developed which is it pn junction is created by doping adjoining areas of a semiconductor with surplus donors and accepters, respectively (Pollock, 1995). This photodiode do not permit photo-detection at high modulation frequency because of its depletion layer capacitance is not enough small (Kasap, 2012). This problem is reduced by introducing other type of photodiode that is PIN photodiode.



Figure 2.12: Various sizes of Si photodiode

Source: (Kasap, 2013)

PIN photodiode is photodiode that composed of p-type semiconductor, intrinsic semiconductor and n-type semiconductor. Jun-ichi Nishizawa and his colleagues invent this kind photodiode in 1950. This photodiode has a thicker depletion region than PN photodiode which make it have the advantages of larger quantum efficiency and lower capacitance. In photovoltaic mode, PIN photodiode offer better long wavelength response over PN photodiode. A PIN photodiode has the ability to detect X-ray and gamma ray photons.

2.5.1 Photodiode Circuits

The reverse biased mode of operation for photodiode is shown in Figure 2.13 (a). In this figure, the function of load resistance R_L in the reverse bias circuit is to act as sampling resistor across which the signal is taken. By assuming steady state operation, the I - V characteristics of the photodiode are demonstrated in Figure 2.13 (b). Note that, negative values that produced by both I and V represent reverse current and voltage. In the dark, small reverse current will escalate with the reverse bias while upon illumination, a photocurrent I_{ph} is produced in the photodiode. Through the responsivity R , this photocurrent is proportional to the incident light power P_o . As illustrated in Figure 2.13 (b), the short circuit current I_{sc} under illumination would be $-I_{ph}$ as the photodiode terminals were shorted.

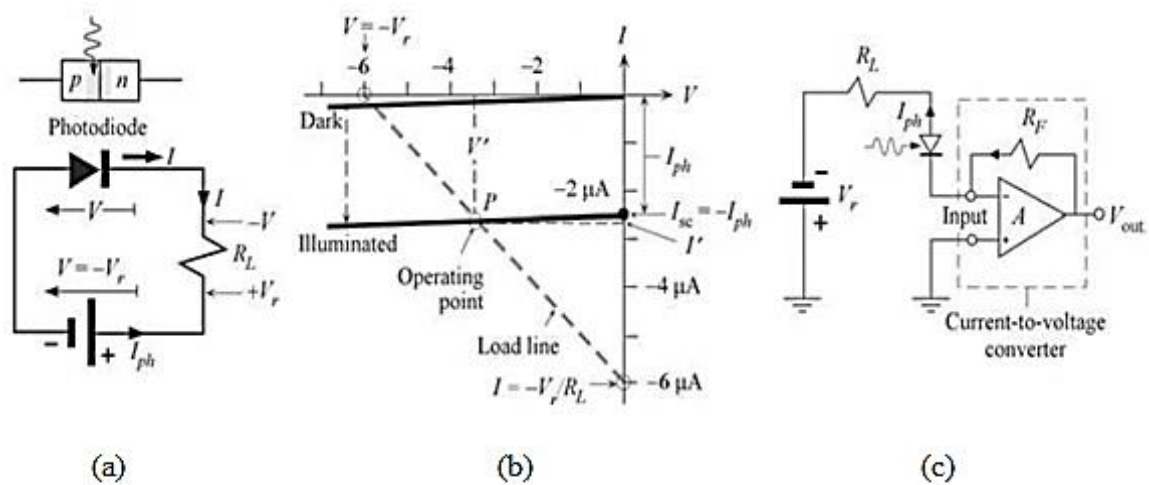


Figure 2.13: Basic operation of photodiode (a) Photodiode in reverse biased (b) I - V characteristics of the photodiode (c) current-voltage converter or a transimpedance amplifier

Source: (Kasap, 2013)

Based on Figure 2.13 (a), the current through R_L obey Ohm's law as in the equation 2.12.

$$I = [(-V) - (+V_r)]/R_L = -(V + V_r)/R_L \quad (2.12)$$

Because of this equation represents the load R on the same axes I and V as the photodiode, it is known as the load line. For $I = 0$, open circuit $V = -V_r$, and it is a point on the load line. For $V = 0$, $I = -V_r/R$, and this is also a point on the load line. The load line then is drawn by pass through these two points as shown in Figure 2.13 (b). The photodiode characteristics at operating point P is cut by this load line. As indicated in Figure 2.13 (b), the current and voltage will be I' and V' .

Note that from Figure 2.13 (b), the magnitude of the operating current I under illumination is very close to the generated photocurrent I_{ph} . This will always happen as long as the photodiode is reverse biased. To convert I_{ph} to output voltage V_{out} , the photocurrent can be redirect into a current-to-voltage converter as in Figure 2.13 (c), in which the output $V_{out} = R_F I_{ph}$. The positive transimpedance gain V_{out}/I_{ph} is determined by the feedback resistor R_F .

CHAPTER 3

METHODOLOGY

3.1 DESIGN AND FABRICATION PROCESS

In the design and development of sedimentation measurement device, there were three main processes that was be implemented. The processes include design and fabrication of mechanical parts, design and fabrication of transmitter-receiver circuit and experimental works. The detail of the processes is shown in the flowchart as in Figure 3.1.

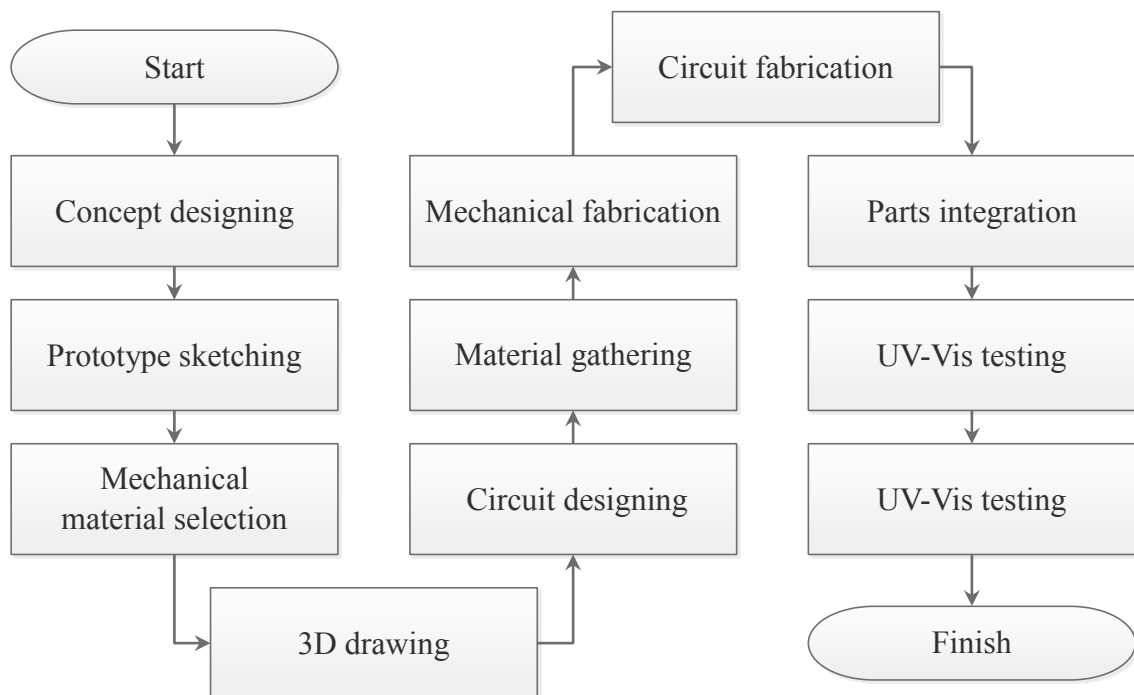


Figure 3.1: Flowchart of research methodology

In the design and fabrication of mechanical parts, the first process that was concept designing. This process was implemented for the purpose of determining how the light transmission can be applied to measure particles sedimentation in MRF. Next, the sketch for the developed device was created. This sketch gives a clearer view about the laser and sensor position. After that, materials selection for mechanical components was done. When the suitable materials were selected, a detailed three dimensional drawing of the prototype was drawn. This detailed drawing was drawn for the purpose of deciding the needed material quantity. Lastly, the mechanical parts were fabricated using the gathered material producing a completed prototype body.

The first step in the design and fabrication process for transmitter-receiver circuit is circuit designing. This step was done in order to decide how the laser and light sensor can be operated. Besides that, the required electronic components were determined through this process. Next, by using the gathered components, the circuit was fabricated. Lastly, the fabricated circuit was installed on the prototype body.

The last process in this project are performing two type of experimental works. These experimental works were done in order to verify the reliability of transmitter-receiver system and to evaluate the functionality of developed prototype.

3.1.1 Design Concept

The design of the sedimentation measuring device is based on light transmission concept. This concept used a laser of known wavelength as light transmitter and a photodiode as light receiver. The laser beam is passed through the MRF sample that filled in the glass tube as shown in Figure 3.2. Then, the light intensity that escape from the sample is collected by the photodiode. The prototype design consists of the base, laser column, sensor column, laser holder, tube holder, sensor holder, laser diode and photodiode. Both laser holder and sensor holder can be vertically move upward and downward for the purpose of alignment.

Figure 3.2 demonstrate the working principle of the prototype. Initially, the sample is assumed dispersed homogeneously within the base fluid. This make the laser hardly to penetrate the sample due to its opaque colour. Because of the laser intensity that exit from the sample is weak, the sensor will absorb lower light power. After several

moments, some of the particles in the sample settle down to the bottom of the vessel. This make the laser penetrate more intense light through the sample. Result from this, the sensor output will increase correspond to the increase of the received light intensity. Finally, the particles in the sample become fully sediment then make the photodiode collect the light at the maximum intensity.

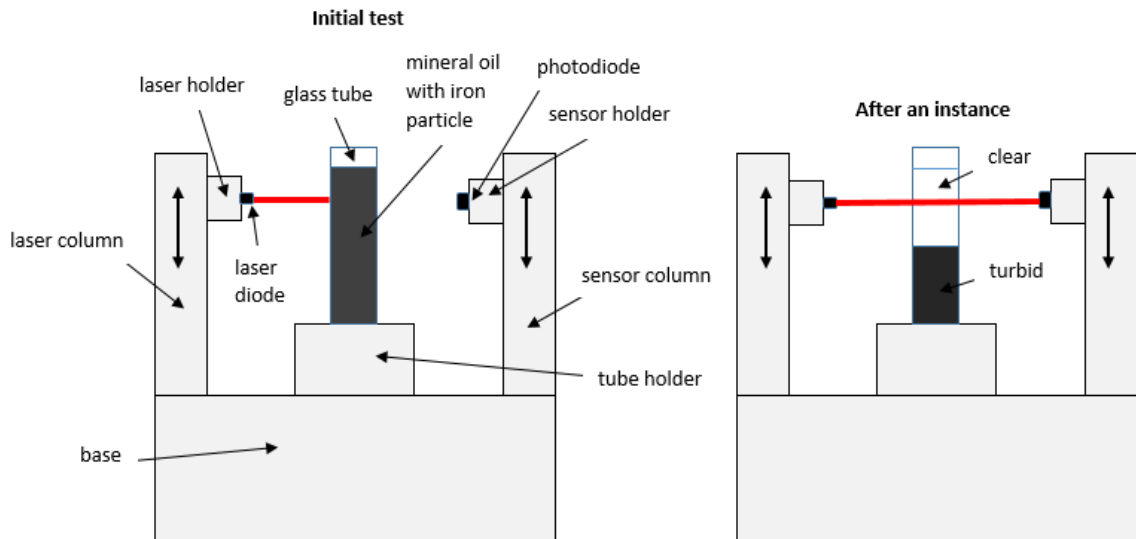


Figure 3.2: Prototype sketching

The photodiode that act as light sensor will translate the light power input to the relative voltage output. So, the voltage output from the sensor will change accordingly to the change of the light intensity. When the suspension become fully sediment, the light power receive from the sensor is not necessarily the same as the light power that omitted by the laser. This is because the light power might be attenuated by the glass tube and the base fluid.

It is assumed that the light intensity after passes through the MRF sample will increase relatively linear to the decrease of particles portion in the transmitted area. By this assumption, the sedimentation ratio, S_r is obtained by

$$S_r = \frac{V_f - V_i}{V_f} \times 100\% \quad (3.1)$$

where, V_i is the initial voltage output of the sensor while V_f is the final voltage output of the sensor.

3.1.2 Prototype Design and Fabrication

The design works of the prototype was begun by sketching a two dimensional drawing as shown in Figure 3.2. Then, the two dimensional drawing was redrawn as three dimensional drawing by using computer aided three-dimensional interactive application (CATIA) as shown in Figure 3.3. As can be seen in Figure 3.3, the overall dimension of the prototype is 250 mm × 135 mm × 175 mm. By referring to this drawing, the materials to be used were decided. Then, the design was redrawn once again as shown in Figure 3.4 in order to determining the required material quantity. This drawing illustrates the real looking of the prototype. Figure 3.5 illustrate the exploded view of the design as well as the components name.

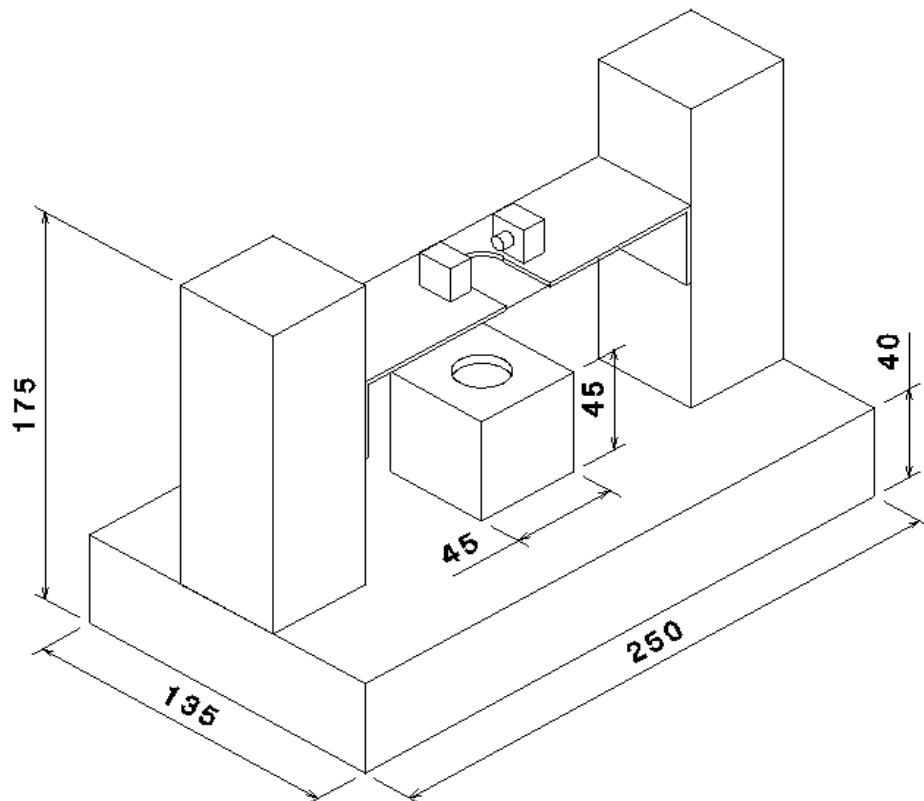


Figure 3.3: An illustration of prototype three dimensional sketching

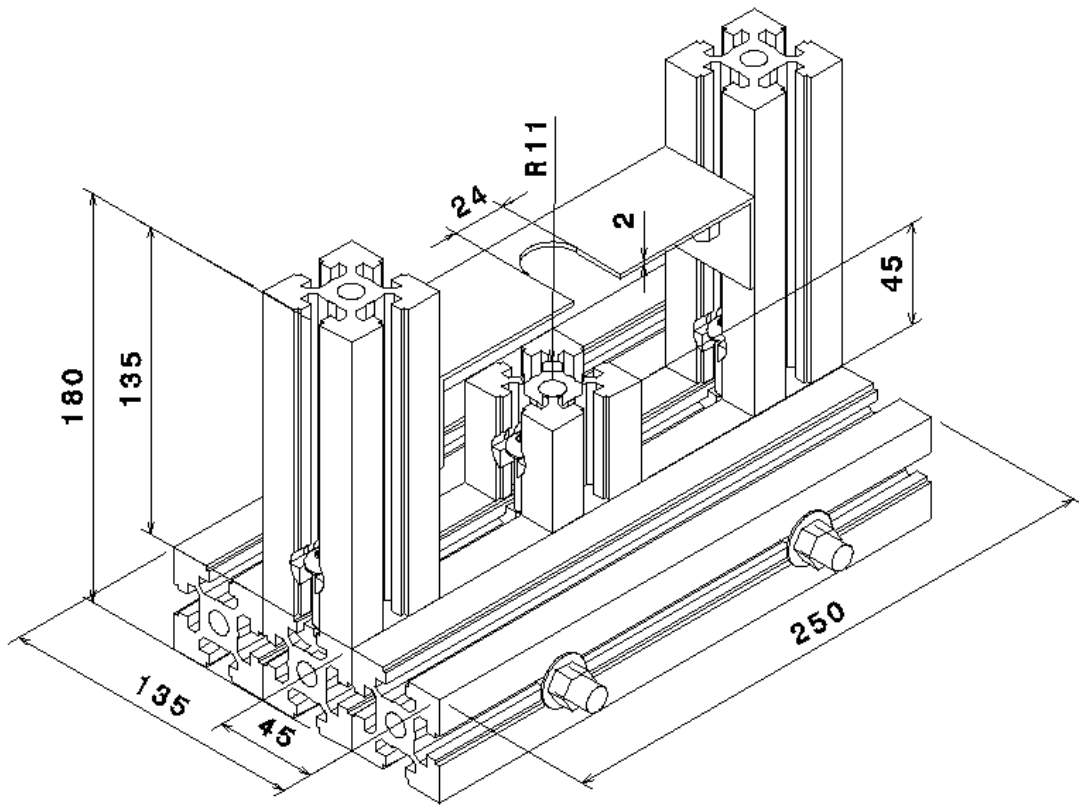


Figure 3.4: Detail prototype design

Figure 3.6 shows the circuit of light transmission-receiving system for the prototype. This system is composed of a sensor circuit and a laser diode circuit. Figure 3.6 (a) illustrate the sensor circuit that run a photodiode in photoconductive mode. With this mode of operation, the photodiode become so sensitive to the changes of received light intensity. As required by this mode, a direct current (DC) voltage was reversely biased to the photodiode.

The photodiode used in this project was BPW21R which is made by Vishay. BPW21R is a planar Silicon PN photodiode with the range of spectral bandwidth of 420 to 675 nm. This photodiode has the peak sensitivity wavelength of 565 nm. This means that, this photodiode will most sensitive to the wavelength of 565 nm. According to the photodiode datasheet, this photodiode can be reverse biased with a 10V DC voltage. DC biasing with greater voltage will cause severe deterioration of the photodiode performance.

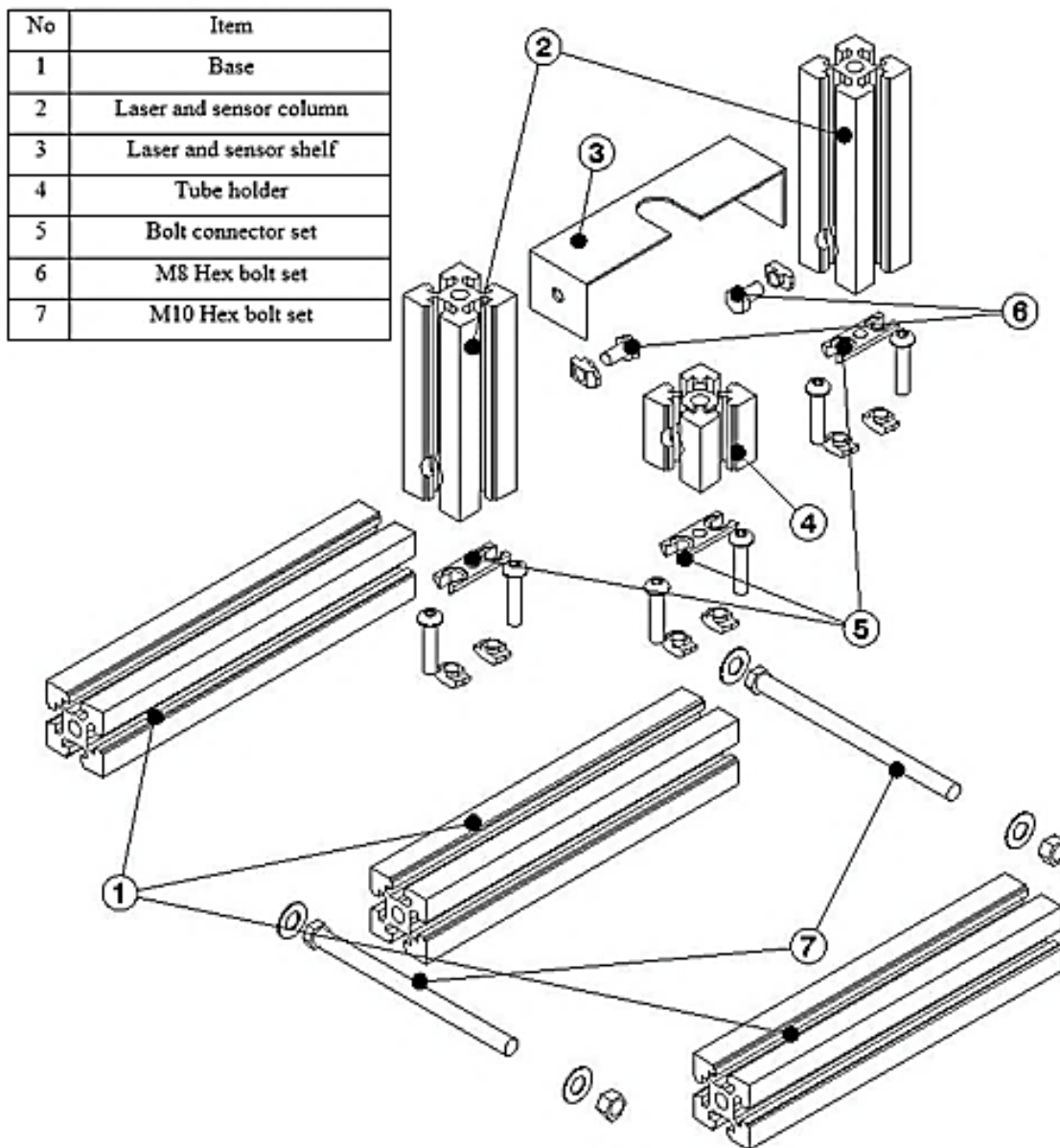
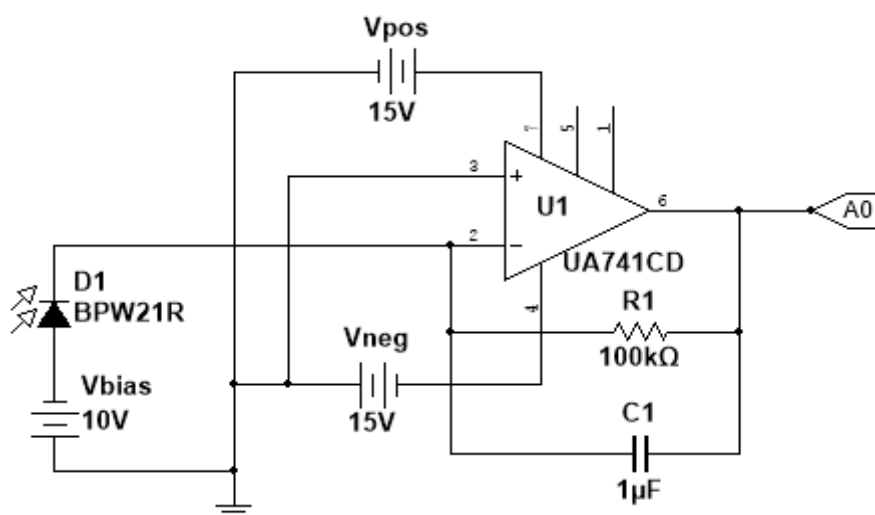


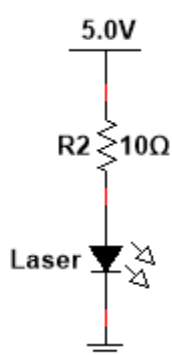
Figure 3.5: An exploded view of prototype design

UA741CD which is a general purpose operational amplifier (OPAMP) was used in this circuit. This electronic device was used so that the small output voltage produce by the photodiode could be amplified. The amplification gain of the output is determined by R_1 . The function of capacitor C_1 is to stabilize the voltage output that to be send to the analogue pin A0 of Arduino Uno. This OPAMP was powered by 15V power supply with dual output.

Figure 3.6 (b) illustrate the simple laser diode circuit used. The wavelength of the laser diode used was 650 nm. The power rating of the laser diode used is 5 mW. The supply voltage of 5V was taken from the Arduino to power up this laser. A 10-ohm resistor was used in order to limit the current flow through the diode. The value of resistor used was chosen based on the allowable operating current of the laser diode. The operating current limit for this laser diode is 0.5 A. The laser diode will be burnt out if it run with current that beyond this allowable operating current.



(a)



(b)

Figure 3.6: Light transmission-receiving system for the prototype (a) sensor circuit, (b) laser diode circuit

Figure 3.7 shows the source code that was written and uploaded to the Arduino. The first two line of source code was written for the purpose variables declaration. The first line of the code named the analogue input pin A0 of the Arduino as “sensorPin”. While the second line assigned a variable “sensorValue” to store the analogue input which is coming from the sensor circuit. The basic requirement code for Arduino to run was also included. The basic code is “setup()” function and “loop()” function.

“Serial.begin(9600)” is a command used in “setup()” function in order to begin the serial communications between Arduino board and computer at 9600 bits of data per second. In the “loop()” block, the “analogRead” command fetched the analogue signal from sensor circuit. Then, the fetched signal was digitized and stored in “sensorValue” variable. The converted digital value has the resolution of 1024. This value is based on the built in 10-bit analogue-to-digital converter (ADC) in Arduino Uno. Next, the stored value was processed and send to computer by using Serial.println() command.

```
int sensorPin = A0; // analog input pin to hook the sensor to
int sensorValue = 0; // variable to store the value coming from the sensor

void setup() {
  Serial.begin(9600); // initialize serial communications
}

void loop() {
  sensorValue = analogRead(sensorPin); // read the value from the sensor
  Serial.println((sensorValue*5.26)/1024); // print to serial
  delay(300000); // 5 minutes time delay
}
```

Figure 3.7: Arduino programming for interfacing with photodiode circuit

The voltage that could be produced by sensor circuit is ranging from 0 V to 5.26 V. To display this range of value on the computer, the generated sensor voltage that available at A0 pin of Arduino was multiply by 5.26V. The result of multiplication then was divided by 1024. This operation was done by using Serial.println((sensorValue*5.26)/1024).

The time interval for Arduino to fetch the output from sensor circuit was 5 minutes. Hence, the Arduino collected 1 data for each intervening period of 5 minutes.

To do this, command “delay(300000) was used in which the 300000 number is the integer value in milisecond. This interger number is equivalent to 5 minutes. This time delay also became the time interval for Arduino to send data to the computer.

The data that send by Arduino to the computer was captured by a simple serial port terminal application that known as CoolTerm. For each 5 minutes, this application received the data from Arduino. This happened according to the time interval that was set in the Arduino source code. Next, the captured data was saved in asc. file format. This kind of file format can be opened via Microsoft Excel for data plotting purpose. Figure 3.8 shows CoolTerm application that was used for data capturing.

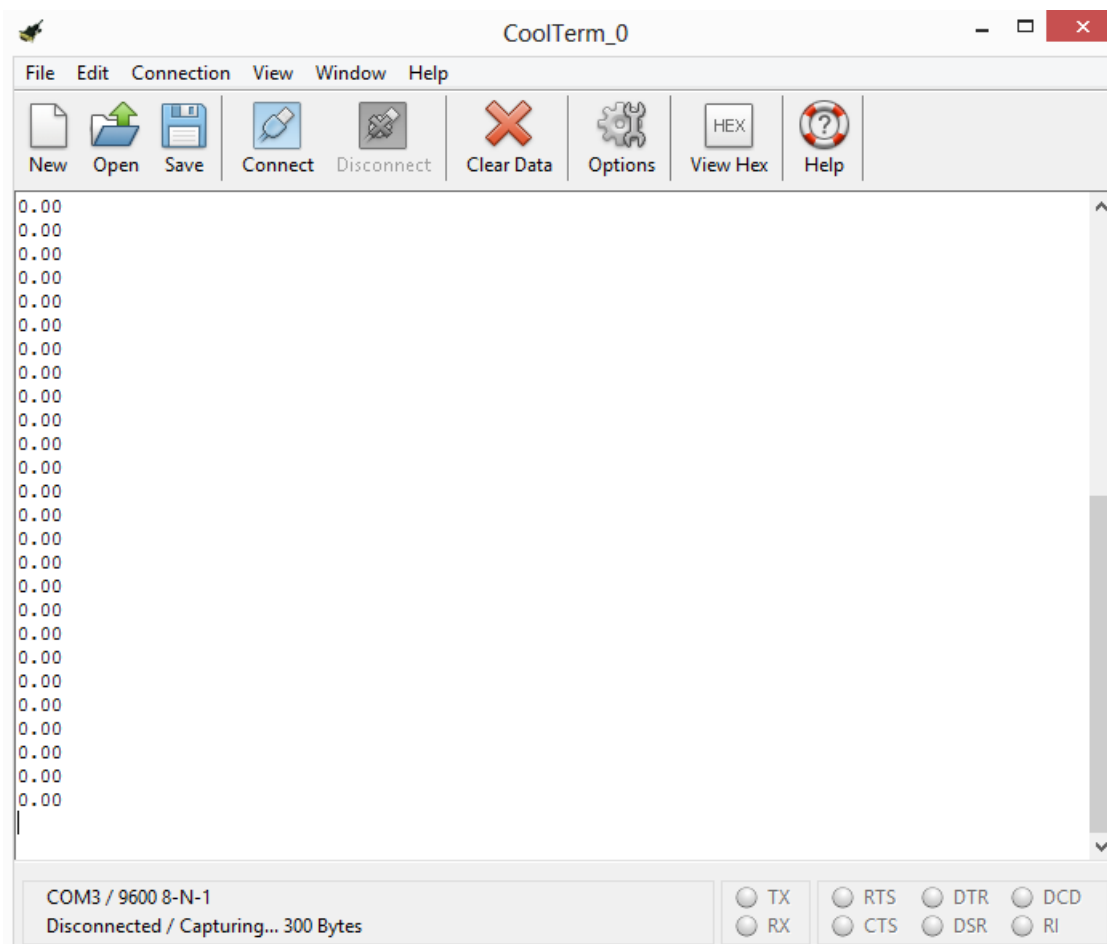


Figure 3.8: CoolTerm application captured the sensor data and saved it in asc. file

3.2 EXPERIMENTAL WORK

The experimental works were comprised of verification experiment and sedimentation experiment. The objective of the verification experiments is to verify the reliability of the light transmission-receiving system for developed prototype. While the objective for the sedimentation experiment is to evaluate the developed device by measuring the sedimentation rate for three different MRF samples.

There are two tests that were included in the verification experiment. A UV-Vis spectrophotometer was used for both tests. The first test was locating the wavelength that produce the highest particle detection level in clear part of three different MRF samples. While the second test was made comparison between the light absorbance of the samples' clear part measured by UV-Vis spectrophotometer and measured by the prototype.

3.2.1 Verification Experiment Using UV-Vis Spectrophotometer

For the first test, three different clear parts of MRF samples were evaluated by varying the wavelength starting from 390 nm until 780 nm. This range of wavelength is known as the visible spectrum (Al-Azzawi, 2007). For this range of wavelength, the UV-Vis spectrophotometer was plotted the graph of absorbance versus wavelength. The peak of the plot was the highest absorbance value that can be measured by the machine. The highest absorbance means the highest the particles detection by the machine photo sensor. Hence, the wavelength that give the highest particle detection was found by referring to this plot.

For the second test, the same three clear parts of MRF samples were used once again in order to measure the absorbance at the wavelength of 650 nm. At this wavelength, the UV-Vis spectrophotometer evaluated the absorbance for these three clear parts. After that, the different between light absorbance of samples' clear part measured by this machine and measured by the prototype was compared. This second test was performed in order to evaluate the reliability of the light sensor of prototype.

Figure 3.9 displays three glass tubes each of which was filled with 20 ml of different MRF. Sample 1 was composed of 20% of CIP, 75% of HO and 5% of SiO₂ while sample 2 was composed of 25% of CIP, 70% of HO, 3.75% of Cu and 1.25% of

SiO₂. Sample 3 was composed of 20% of CIP, 75% of HO and 5% of Cu. Table 3.1 summarizes all these samples with more detail information. As can be seen in Figure 3.9, the upper part of each sample is the clear part of MRF that exist after particles sedimentation. All samples in this figure are in the state of fully particles sedimentation.

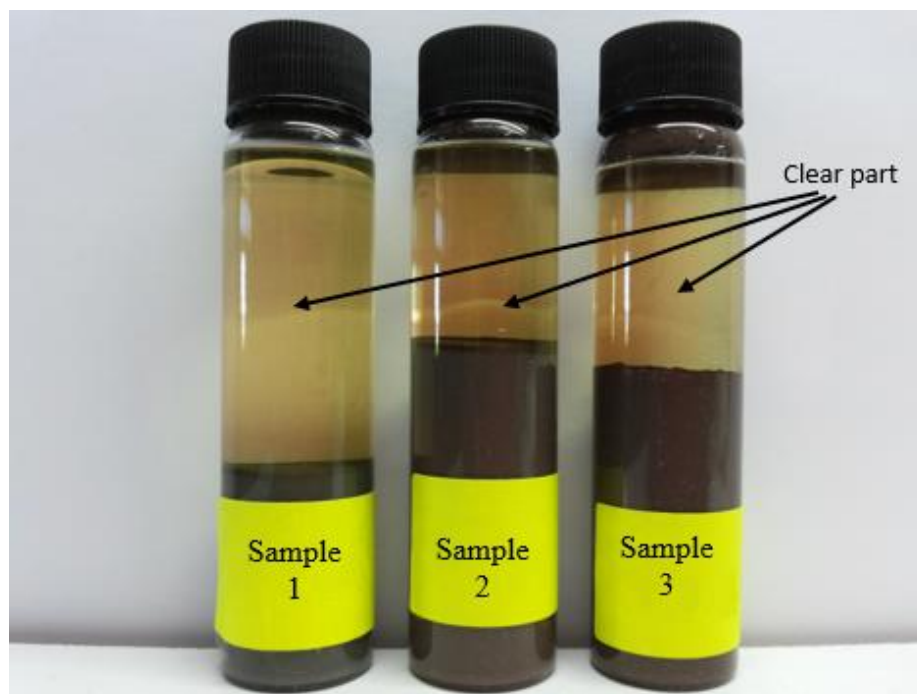


Figure 3.9: Three different MRF samples

Table 3.1: Sample with different component composition and their volume percentage

| Sample | Component | Density (g/mL) | Vol% | mL | g |
|--------|------------------|----------------|------|------|--------|
| 1 | CIP | 7.86 | 20 | 12 | 94.32 |
| | HO | 0.874 | 75 | 45 | 39.33 |
| | Cu | 8.94 | 0 | 0 | 0.00 |
| | SiO ₂ | 0.037 | 5 | 3 | 0.11 |
| 2 | CIP | 7.86 | 25 | 15 | 117.90 |
| | HO | 0.874 | 70 | 42 | 36.71 |
| | Cu | 8.94 | 3.75 | 2.25 | 20.12 |
| | SiO ₂ | 0.037 | 1.25 | 0.75 | 0.03 |
| 3 | CIP | 7.86 | 20 | 12 | 94.32 |
| | HO | 0.874 | 75 | 45 | 39.33 |
| | Cu | 8.94 | 5 | 3 | 26.82 |
| | SiO ₂ | 0.037 | 0 | 0 | 0.00 |

Figure 3.10 indicates the UV-Vis spectrophotometer (GENESYS™ 10S) used in the two verification experiments. The function of this device is to measure the amount of light absorbed by a solution. With this measurement, the concentration of a solution can be known. This instrument can perform the absorbance measurement at any single wavelength that range from 190 to 1100 nm. Using the same range of wavelength, this device also able to do absorbance scanning. The absorbance data that collected by this machine is displayed on the LCD screen. The data also can be transferred and saved in USB flash drive.



Figure 3.10: An UV-Vis spectrophotometer model GENESYS™ 10S

In order to perform the absorbance measurement using UV-Vis spectrophotometer, the clear part of each MRF samples were drawn after 12-hours of particles sedimentation. By using pipette, each sample's clear part was transferred from glass tube to 1 cm plastic cuvette (Figure 3.12). As a precaution, it was ensured that the creaming part of the MRF samples that exist at the meniscus were not sucked along with

the clear part. Figure 3.11 illustrates the three different parts that existed after particle sedimentation.

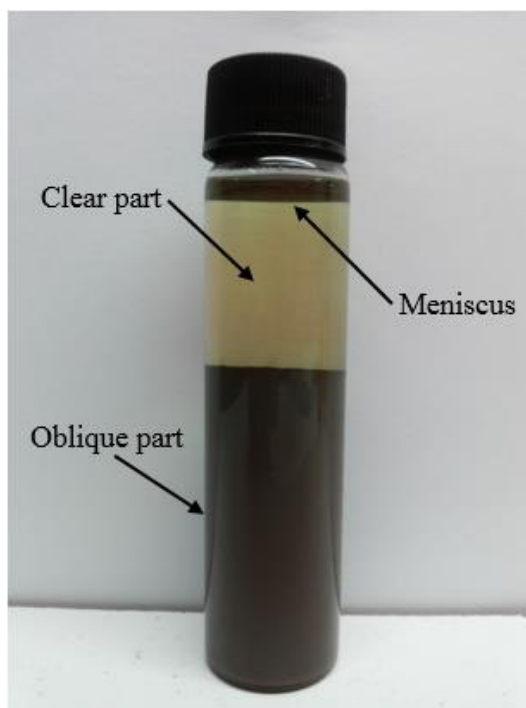


Figure 3.11: An illustration of three different parts that existed after particle sedimentation

Before the absorbance scan of the clear part of samples were started, the absorbance of the hydraulic oil as the blank was measured as zero absorbance. This step was done because, the spectrophotometer need a reference absorbance value in order to give reading to other samples. Then, the absorbance scan was done in the range of visible light spectrum which is starting from 390 nm to 780 nm wavelength. The data obtained then was saved in USB flash drive so that it could be transferred into computer. By using Microsoft Excel, the data collected was plotted and analysed. Absorbance measurement at the wavelength 650 nm also performed for all samples. The results are tabulated in Table 4.1.

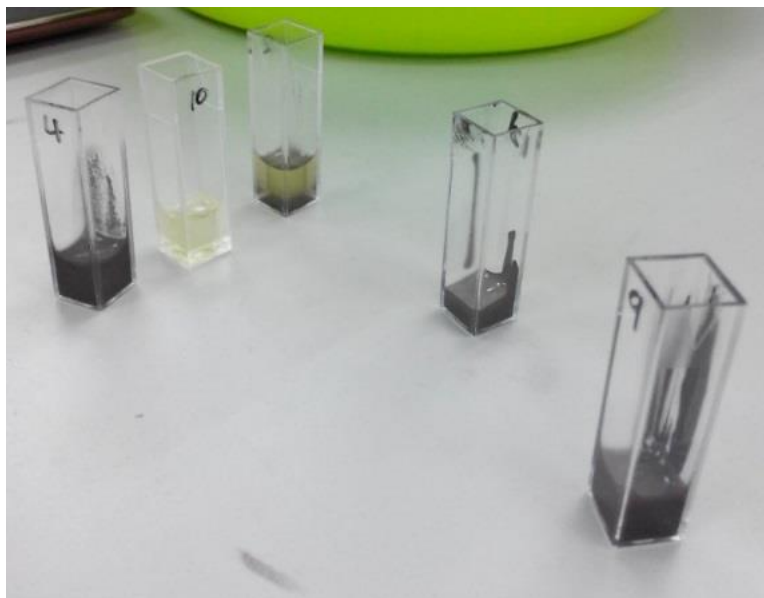


Figure 3.12: 1 cm × 1 cm plastic cuvette that was used to hold the samples' clear part in order to examine using UV-Vis spectrophotometer

3.2.2 Sedimentation Experiment Using the Developed Prototype

For the last part of the experimental works, the developed device was evaluated by conducting sedimentation analysis for three different MRF samples. The composition for each MRF samples used are tabulated in Table 3.1. Figure 3.12 illustrate the developed prototype was performing the sedimentation monitoring. The prototype was configured to measure the sedimentation at a single spot of the sample that is exactly below the meniscus level of the samples.

Before the MRF samples were examined, the meniscus of each samples were recognized. To get the location of the meniscus, the particles in each samples were homogeneously dispersed in the carrier fluid. This step was done by shaken the samples by hand. Next, the samples were leave to sediment until the meniscus can be observed. After the location of the meniscus was found, the samples were placed at the tube holder of the prototype. Then, the laser beam was directed exactly under the meniscus level.

To start the sedimentation measurement, the samples were shaken once again. It was ensured that the samples were shaken until the iron particles is homogeneously dispersed in the carrier fluid. This measurement was done without the absence of external

magnetic field around the MRF samples. After the experiment done, the collected results were plotted by using Microsoft Excel as shown in Figure 4.3.

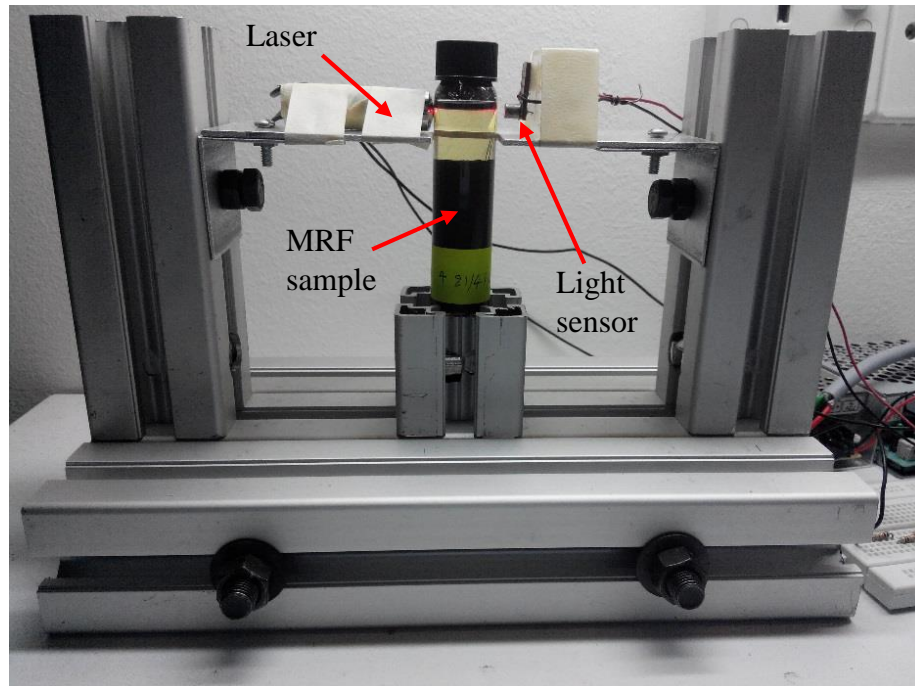


Figure 3.13: Sedimentation rate of a sample is being tested

CHAPTER 4

RESULT AND DISCUSION

4.1 FABRICATED PROTOTYPE OF SETTLING MONITORING DEVICE

Figure 4.1 shows the result from the fabrication works of the sedimentation measurement device. This device is comprised of a laser, a light sensor, a bracket, a tube holder, a base and two columns. The bracket that hold the laser and sensor can be move upward or downward. This movement can be done by loosen the black screws. In addition, the tube holder also can be moved but in different direction. This holder can be move to the left or to the right.

This prototype mostly is made out of aluminium profile. The aluminium profile was used to make the base, the columns and the tube holder. For the laser-sensor bracket, it was made out of aluminium plate. The used of aluminium makes the prototype become easy to be move anywhere. Moreover, the corrosion resistance characteristic possess by aluminium makes the prototype become long lasting. The all components of the prototype were combined by using bolts and nuts.

Figure 4.2 demonstrates the fabricated circuit of transmitter-receiver system. This system applies the principle of light transmission through medium. The circuit in Figure 4.2 is composed of Arduino, sensor circuit and laser circuit. The circuit that bordered by the yellow line is the sensor circuit. While, the circuit that bordered by the red line is the laser circuit. The OPAMP in the sensor circuit can be easily removed from the socket. The OPAMP is intentionally be connected in this way to the circuit. This way of connection is for the purpose OPAMP replacement when it broken.

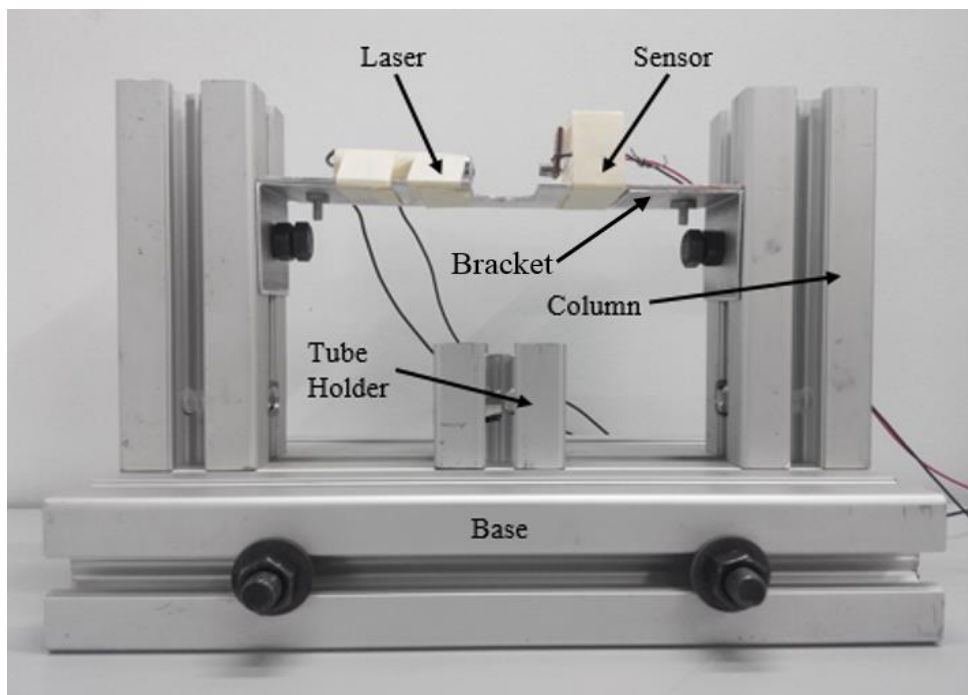


Figure 4.1: A photo of completed prototype

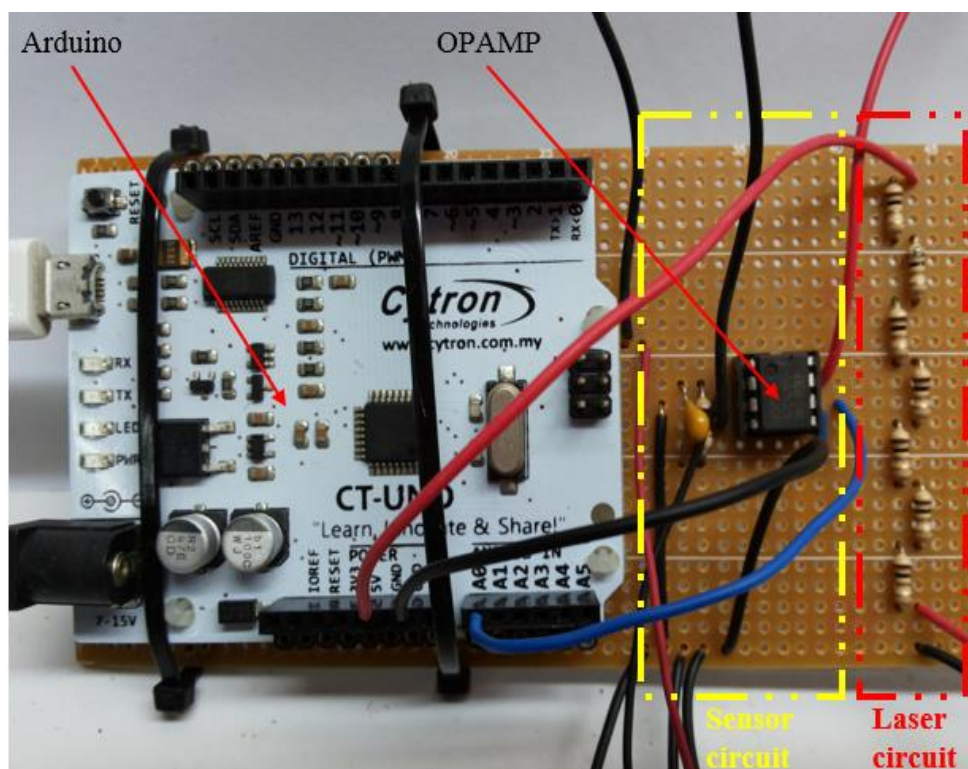


Figure 4.2: A photo of completed circuits

4.2 VERIFICATION EXPERIMENT RESULTS AND DISCUSSION

Figure 4.3 shows the results of the first test of verification experiment. This figure shows the absorbance readings for the clear part of each MRF samples produced by the UV-Vis spectrophotometer. These measurements were taken by varying the light source wavelength of the machine from 390 nm to 780 nm. The green line is the absorbance plot for sample 1. While the red line indicates the absorbance plot for sample 2. For sample 3, its absorbance plot is shown by the blue line. Sample 1 is composed of 20% of CIP, 75% of HO and 5% of SiO₂ while sample 2 is composed of 25% of CIP, 70% of HO, 3.75% of Cu and 1.25% of SiO₂. The composition of sample 3 is 20% of CIP, 75% of HO and 5% of Cu.

Absorbance is a dimensionless quantity that measure how much light absorbed by a solution. In term of mathematical definition, absorbance and transmittance are logarithmically related. The transmittance T is defined as

$$T = \frac{P}{P_L} \quad (4.1)$$

where, P is radiant power emitted by the light source, and P_L is the radiant power leaving the sample. While, absorbance A is defined as the negative base-10 logarithm of a transmittance as shown in the equation 4.2 (Ball, 2001).

$$A = \log_{10} \left(\frac{1}{T} \right) \quad (4.2)$$

Based on Beer – Lambert law in equation 4.3 , the absorbance is related to the length of the light-path l which is the diameter of the sample glass tube, molar absorption coefficient ε of the solution, and concentration c of the solution (Gore, 2000).

$$A = \varepsilon cl \quad (4.3)$$

Because of the light-path l and the molar absorption coefficient ε are constant, the absorbance only related with the solution concentration. For the result in Figure 4.3, it

shows that the more the absorbance reading the more concentrate the particles absence in the samples' clear part.

According to the graph in Figure 4.3, it can be seen that the trend of the three plots are almost the same. This means that there is no significant optical property different among the three samples. For sample 1, the absorbance increases with the increasing of the wavelength starting from 390 nm until its peak of absorbance at 411 nm. When the plot goes beyond the wavelength of 411 nm, the absorbance gradually decreases until the final spectra. While for sample 2 and sample 3, the absorbance reading also increase at the initial wavelength till to their peak of absorbance. The peak of absorbance for these two samples are 419 nm and 421 nm respectively.

The plots in Figure 4.3 happened because of the effect of quantum process. This is the process of how light interact with matter. It is known that when light passing through a solution, the absorbance of the light to that solution can be caused by absorption. The absorption of a photon will take place only when the quantum energy, E of the photon exactly the same magnitude as the energy difference between the ground and maximum excited states of the solution's atom or molecule. Figure 4.4 demonstrates how the absorption of a photon of matter is happened.

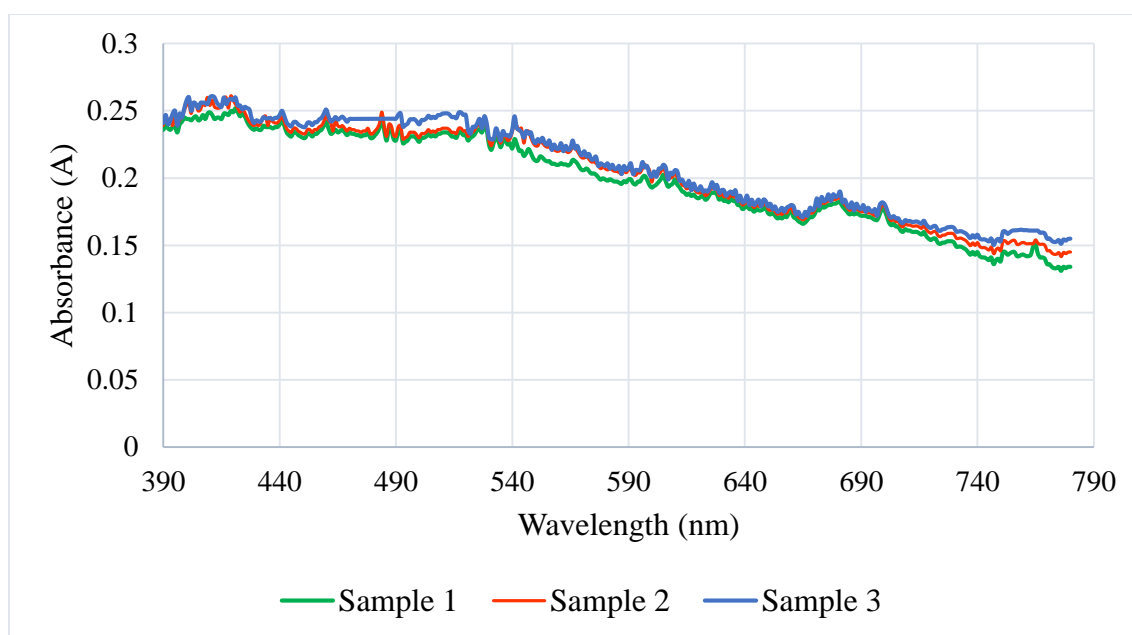


Figure 4.3: Absorbance reading by UV-Vis spectrophotometer with variation of wavelengths (390 nm-780 nm)

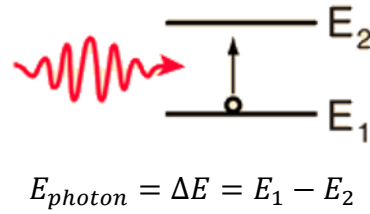


Figure 4.4: An illustration of light absorption process of a matter

According to the plank equation, quantum energy of a photon is inversely proportional to its light wavelength as shown in equation 4.4

$$E_{\text{photon}} = \frac{hc}{\lambda} \quad (4.4)$$

where, the plank constant $h = 4.136 \times 10^{-15} \text{ eV}\cdot\text{s}$ and the speed of light, $c = 3 \times 10^8 \text{ ms}^{-1}$. Hence, different electromagnetic wavelength produces different photon energy. By correlating this equation with the graph in Figure 4.3, it can be concluded that the wavelength at peak of absorbance reading is the most suitable wavelength to transmit through MRF samples in order to detect the appearance of particles in the carrier fluid.

Table 4.1 shows the results for the second test of verification experiment. This table records the absorbance reading for three samples' clear part by the UV-Vis spectrophotometer at the wavelength of 650 nm. The result obtained by the prototype at the same wavelength is also included in this table. For absorbance value that measure by UV-Vis spectrophotometer, sample 3 shown the highest absorbance value while sample 1 shown the lowest absorbance value. Unfortunately, the developed prototype did not give any absorbance value.

The prototype did not give the absorbance value directly. The prototype only gives the output in term of voltage value. This voltage output was used to get the absorbance value by calculation. This calculation was done by using the equation 4.1 and 4.2. The voltage reading by the sensor when measuring the laser intensity passes through the clear part of the three samples was 5.26V. While the sensor voltage reading when measuring the laser intensity without passes through those clear parts was also 5.26V. This means that there is no light attenuation that can be detected by the sensor after the radiated light passes through the fluid. So, the emitted radiant power, P was simply the same as the

radiant leaving the sample, P_L . Thus, the absorbance value for the three samples' clear part is the same that is $A = \log_{10}(1) = 0$. This happened probably due to the peak sensitivity of the photodiode used do not match with the wavelength of the laser used.

Table 4.1: Absorbance comparison between UV-Vis spectrophotometer and prototype

| Sample | Absorbance at 650 nm | |
|--------|----------------------|-----------|
| | UV-Vis | Prototype |
| 1 | 0.174 | 0 |
| 2 | 0.177 | 0 |
| 3 | 0.179 | 0 |

4.3 SEDIMENTATION EXPERIMENT RESULTS AND DISCUSSION

Figure 4.5 shows the sedimentation measurement results for three different MRF samples. The graph of sedimentation ratio against period in Figure 4.5 was plotted by using Microsoft Excel. The sedimentation of the three samples were examined by using the developed prototype within 24-hours. Before the samples were examined, it was ensured that the particles in all samples were homogeneously dispersed. The sedimentation ratio for each MRF sample was tested at the absence of external field.

In Figure 4.5, the green line represents the sedimentation behaviour for sample 1. While the red line shows the sedimentation plot for sample 2. The sedimentation ratio for sample 3 is represented by the blue line. The vertical-axis of the graph is the voltage ratio percentage while the horizontal-axis of the graph is the period (minute). The sedimentation ratios of the graph were calculated by using the equation (3.1). In this equation, sedimentation ratio is equal to the ratio of different between final voltage and initial voltage to the final voltage. The initial voltage readings for three samples were 0 V and the final voltage readings were 5.26 V.

From the Figure 4.5, the all sedimentation plots of the developed prototype show the same trend. However, it can be clearly seen that each plot shows different starting point and final point of particles sedimentation. By examining the slope for each plot, it

can be seen that all samples show inconsistent gradient line. This trend is illustrated in more clear view as shown in Figure 4.6, Figure 4.7 and Figure 4.8.

Figure 4.6 shows the plot of sedimentation ratio for MRF sample 1. From this figure, sample 1 that composed of 20% of CIP, 75% of HO and 5% of SiO_2 gives two different rates of sedimentation. The first slope (60 min to 75 min) shows that the particles in this sample sediment with the rate of 1.57 % / minute. While the second slope (75 min to 85 min) shows that the rate of sedimentation become faster which is 7.64 % / min.

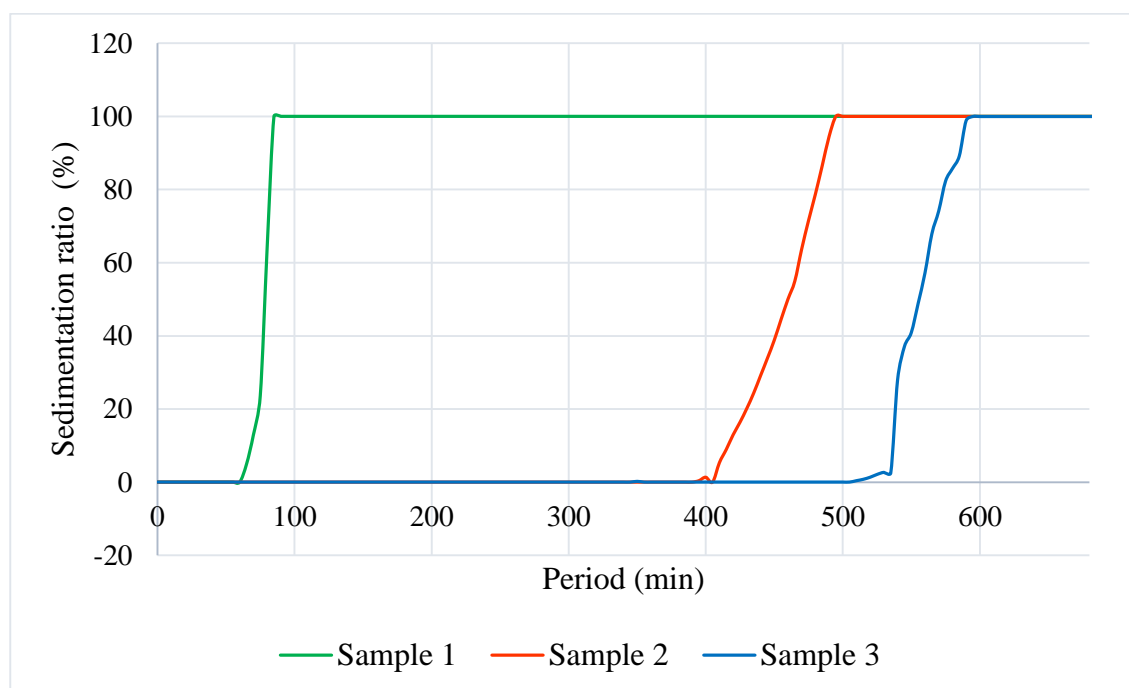


Figure 4.5: Sedimentation ratio measurement by using developed prototype

By referring to the graph in Figure 4.7, particles in sample 2 also sediment with two different speed. Sample 2 that composed of 25% of CIP, 70% of HO, 3.75% of Cu and 1.25% of SiO_2 initially sediment at the rate of 0.9 % / min. The second slope on this graph shows when the period reach at the minute of 465, the sedimentation rate become faster which is 1.51 % / min. This rate of sedimentation is steady until the period of 495.

In Figure 4.7, it can be observed that sample 3 also experience the same sedimentation behaviour as sample 1 and sample 2. With the composition of 20% of CIP, 75% of HO and 5% of Cu, the first slope (505 min to 540 min) shows that this sample initially sediment at rate of 0.51 % / min. Afterward, the sedimentation become faster

which is at the rate of 1.37 % / min. This rate is unchanged until the final measurement as shown by the second gradient line (540 min to 595 min).

By comparing the slope among the three MRF samples, sample 1 shows the highest sedimentation rate. This shows that the additive (SiO_2) used for this sample did not give much aid in order to make the solid particle suspend longer in the carrier fluid. In comparison, sample 2 become the second faster of sedimentation rate. These indicate that the Cu and SiO_2 contained in sample 2 give much longer particles' suspension time. It is obvious that, the best MRF sample is sample 3 which give the lowest sedimentation rate. This explained that, the use of Cu is already enough to lower the sedimentation time.

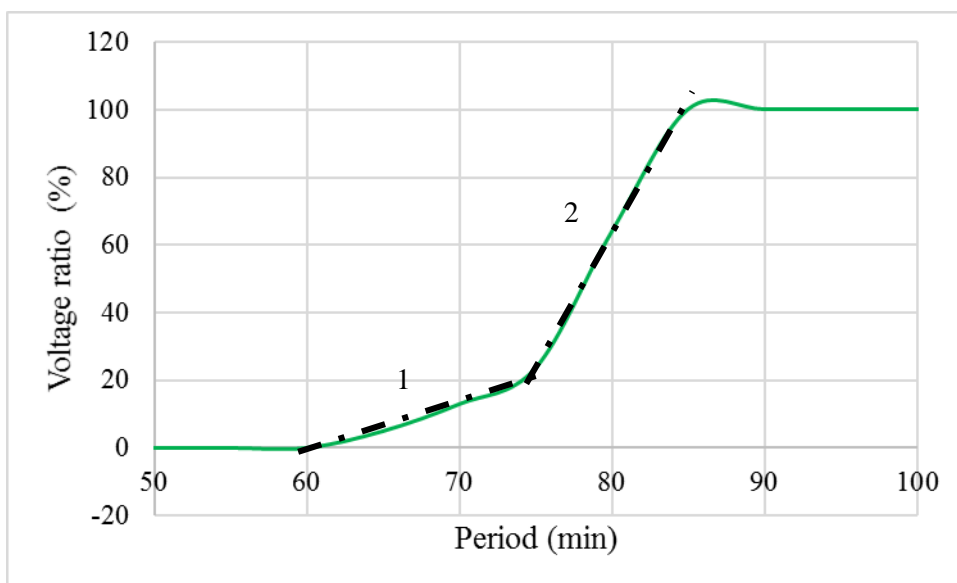


Figure 4.6: The magnified view of sedimentation plot for sample 1

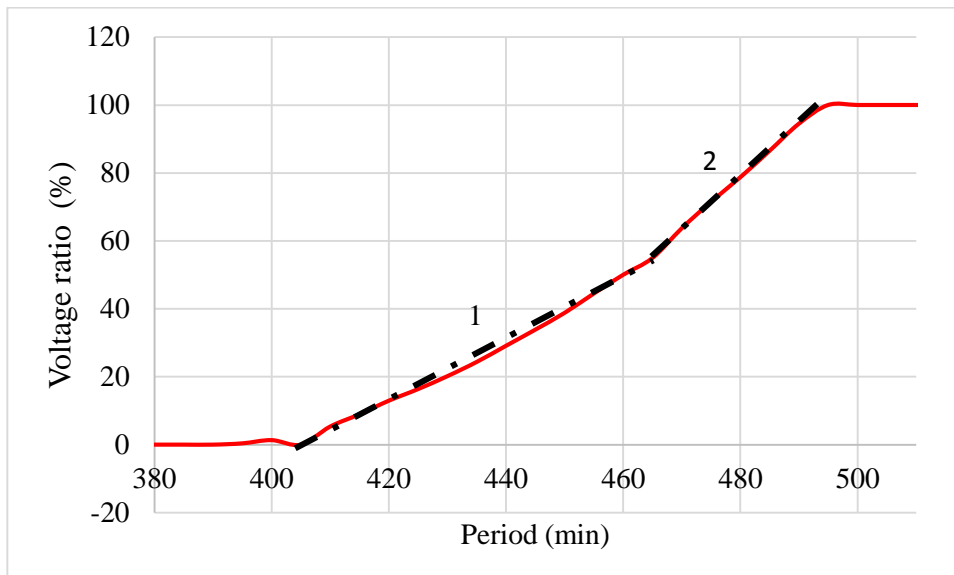


Figure 4.7: The magnified view of sedimentation plot for sample 2

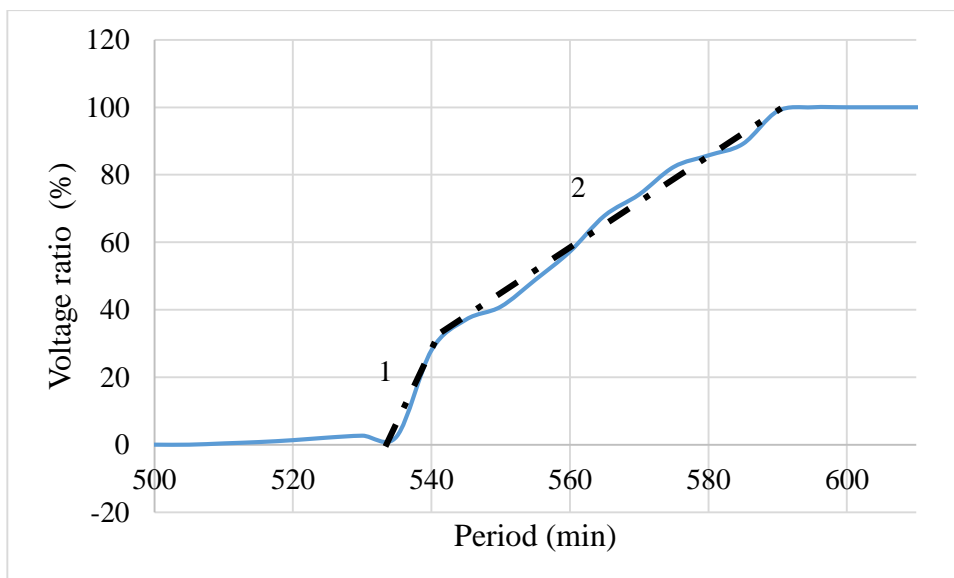


Figure 4.8: The magnified view of sedimentation plot for sample 3

The trend line of the graph in Figure 4.5 can be explained by referring to Figure 4.9. Figure 4.9 shows how the particles sediment in one of MRF sample that was tested. In Figure 4.9, it can be observed that the clear part of the sample become bigger as time goes. There is an interface that exist between the clear part and the oblique part. This interface is called as mudline. The rate of particles sedimentation was monitor by the

prototype based on the downward movement of this mudline. This mudline exists due to the compression mode of sedimentation (Azema, 2006). In this mode of sedimentation, the particles form strong bonding between each other. This bonding make the particles sediment in clusters (Abel, Stangle, Schilling, & Aksay, 1994). Because if this event, there is no particles can be between the mudline and the meniscus of the sample.

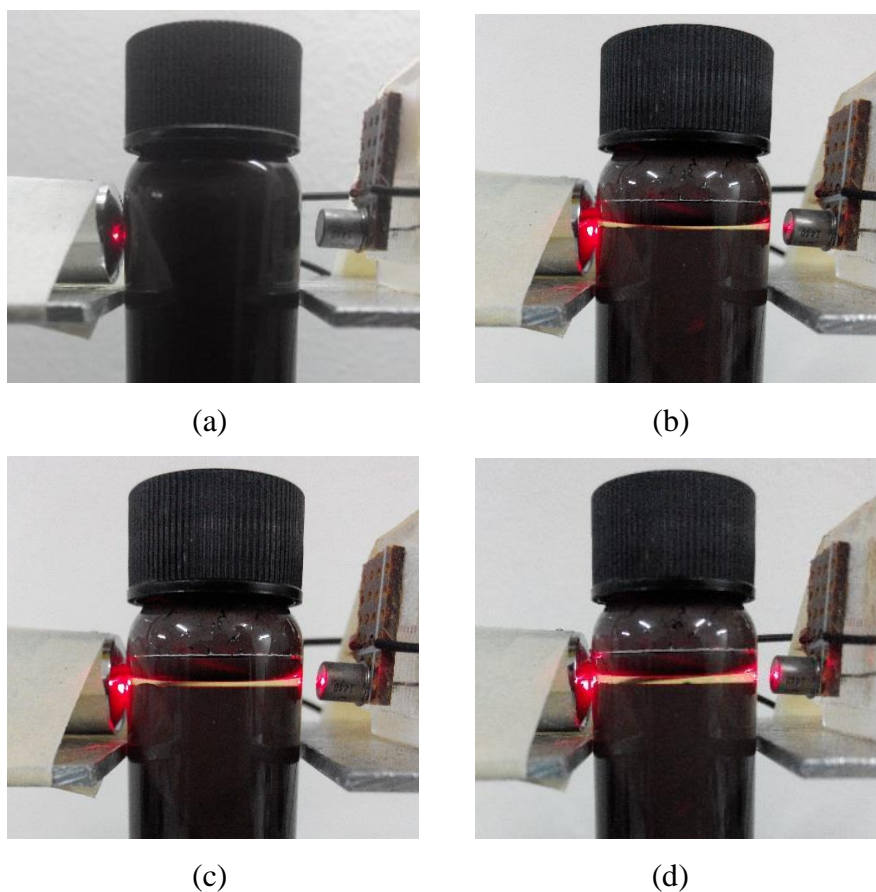


Figure 4.9: A photo of sample 2 (a) Initial experiment, (b) minute of 395, (c) minute of 428 and (d) final experiment

CHAPTER 5

CONCLUSION AND RECOMMENDATION

5.1 CONCLUSION

In the development of materials of suspension, one of the important aspects to be refined is stability. Higher stability resulting in a better performance of suspension. Various methods have been used by many developers to analyse the stability. However, the methods used have their drawbacks. For example, the visual inspection method produces the results with poor accuracy because of observer's parallax error. Meanwhile, digital photography methods need proper lighting in order to obtain good image before it can be processed. Therefore, other methods should be established in order to overcome those weaknesses.

A sedimentation measurement device for MRF was designed and developed based on the concept of light transmission method. For the light transmission-receiving system of the device, a red laser diode (650 nm) was used as light transmitter and a photodiode was used as light receiver. Transimpedance amplifier was implemented for driving the sensor circuit. Furthermore, an Arduino microcontroller was used as an interface between the computer and the sensor circuit of the prototype. Most of the mechanical parts was made out of aluminium profiles due to its light weight and non-corrosive behaviour.

The reliability of the light transmission-receiving system was evaluated by performing two experiments. The first experiment was done by locating the wavelength that could produce the highest particles detection level in clear part of three different MRF samples. The first sample was composed of 20% of CIP, 75% of HO and 5% of SiO₂ while the second sample was composed of 25% of CIP, 70% of HO, 3.75% of Cu and 1.25% of SiO₂. The third sample was composed of 20% of CIP, 75% of HO and 5% of

Cu. By using UV-Vis spectrophotometer, the absorbance measurement was done by varying the wavelength starting from 390 nm to 780 nm. The result for this experiment suggest that the maximum absorbance value of clear part for the three MRF samples was achieved at the wavelength ranging from 411 nm to 421 nm. Hence, these wavelengths give the highest particles detection in that clear parts.

For the second experiment, the evaluation of the light transmission-receiving system was done by comparing between the light absorbance of clear part of the samples measured by UV-Vis spectrophotometer and measured by the developed device. By using the same machine as in the first experiment, the absorbance reading of clear part of the three MRF samples was obtained at the wavelength of 650 nm. Then, the absorbance value once again was measured by using the prototype. Lastly, these two measurement results were compared. The outcome from the comparison indicate that the light detector used in the prototype could not give the same detection sensitivity as the light detector of the UV-Vis spectrophotometer. This weakness is caused by the mismatch between the laser wavelength and the photodiode peak sensitivity wavelength.

The evaluation of the developed device was done by conducting the sedimentation analysis for three different MRF samples. By using the same MRF samples that were used in the two verification experiment for light transmission-receiving system, the sedimentation behaviour of these samples were monitored by the prototype. The evaluation result presents that the prototype was able to carry out the sedimentation monitoring for the samples.

5.2 RECOMMENDATION

There are several modifications that can be implement to the design of the prototype. These modification is needed so that the reliability of developed device can be improved. The first modification is replacing the laser (650 nm) used with other laser that possess the wavelength ranged between 411 nm and 421 nm. These ranges of wavelength will give the maximum absorbance value at the clear part of MRF samples. Consequently, the particles movement in the MRF samples can be detected with more sensitive.

For the purpose of increasing the sensitivity of particles detection in MRF samples, the replacement of the laser is insufficient. The compatibility between photodiode peak sensitivity wavelength and laser wavelength is also need to considered. As a suggestion, the photodiode used should be changed with other photodiode that have the peak sensitivity wavelength ranged between 411 nm and 421 nm. This specification will make the prototype give more accurate sedimentation measurement result.

To commercialize the developed prototype, other improvement should be added by considering the sustainable development elements. In terms of society, the prototype need to ensure the user's safety and health. For example, the laser light used in the prototype should not be exposed to the user by adding appropriate shield. It is important to reduce the energy consumption of the developed device. For this purpose, the circuit should be redesign with the emphasis more on energy optimization. Lastly, manufacturing method to be implement should be considered in the development process of the prototype. This consideration will eliminate or at least reduce the manufacturing error.

REFERENCES

- Abel, J. S., Stangle, G. C., Schilling, C. H., & Aksay, I. A. (1994). Sedimentation in flocculating colloidal suspensions. *Journal of materials research*, 9(02), 451-461.
- Al-Azzawi, A. (2007). Photonics: Principles and Practices. *Photonics: Principles and Practices*, by Abdul Al-Azzawi. ISBN-10 0-8493-8290-4 (HB); ISBN-13 978-0-8493-8290-1 (HB). Published by CRC Press, Taylor & Francis Group, Boca Raton, FL USA, 2007., 1.
- Azema, N. (2006). Sedimentation behaviour study by three optical methods—granulometric and electrophoresis measurements, dispersion optical analyser. *Powder technology*, 165(3), 133-139.
- Ball, D. W. (2001). *The basics of spectroscopy* (Vol. 49): Spie Press.
- Dobias, B., Qiu, X., & von Rybinski, W. (1999). *Solid-liquid dispersions* (Vol. 81): CRC Press.
- Gore, M. G. (2000). Spectrophotometry and spectrofluorimetry: a practical approach.
- Hazzab, A., Terfous, A., & Ghenaim, A. (2008). Measurement and modeling of the settling velocity of isometric particles. *Powder technology*, 184(1), 105-113.
- Jenkins, F. A., & White, H. E. (2001). Fundamentals of optics.
- Kasap, S. O. (2012). *Optoelectronics & Photonics: Principles & Practices*: Pearson Higher Ed.
- Kasap, S. O. (2013). *Optoelectronics & Photonics: Principles & Practices: International Edition*: Pearson Higher Ed.
- Kciuk, M., & Turczyn, R. (2006). Properties and application of magnetorheological fluids. *Journal of Achievements in Materials and Manufacturing Engineering*, 18(1-2), 127-130.
- Kumar, A., & Mangal, S. (2013). Synthesis of Magneto Rheological Fluid. *Int J Mech Eng Rob Res*, 2(6), 20-25.

- López-López, M., Zugaldía, A., González-Caballero, F., & Durán, J. (2006). Sedimentation and redispersion phenomena in iron-based magnetorheological fluids. *Journal of Rheology (1978-present)*, 50(4), 543-560.
- Mallik, A. K. (2013). Photodiode. *Himalayan Physics*, 4, 95-98.
- Murshed, S., Leong, K., & Yang, C. (2008). Thermophysical and electrokinetic properties of nanofluids—a critical review. *Applied Thermal Engineering*, 28(17), 2109-2125.
- Ogendal, L. (2013). *Light Scattering Demystified Theory and Practice*.
- Petschnigg, G., Szeliski, R., Agrawala, M., Cohen, M., Hoppe, H., & Toyama, K. (2004). Digital photography with flash and no-flash image pairs. *ACM transactions on graphics (TOG)*, 23(3), 664-672.
- Pollock, C. R. (1995). *Fundamentals of optoelectronics*: Irwin.
- Prekas, K., Shah, T., Soin, N., Rangoussi, M., Vassiliadis, S., & Siores, E. (2013). Sedimentation behaviour in electrorheological fluids based on suspensions of zeolite particles in silicone oil. *Journal of colloid and interface science*, 401, 58-64.
- Quimby, R. S. (2006). *Photonics and lasers: an introduction*: John Wiley & Sons.
- Rabbani, Y., Ashtiani, M., & Hashemabadi, S. H. (2015). An experimental study on the effects of temperature and magnetic field strength on the magnetorheological fluid stability and MR effect. *Soft matter*, 11(22), 4453-4460.
- Serway, R., & Jewett, J. (2013). *Physics for scientists and engineers with modern physics*: Cengage learning.
- Xu, Z.-D., Guo, W.-Y., & Chen, B.-B. (2014). Preparation, Property Tests, and Limited Chain Model of Magnetorheological Fluid. *Journal of Materials in Civil Engineering*, 04014229.
- Zhou Feng*, L. Y., Ren Hongjuan. (2015). Study of Sedimentation Stability of Magnetorheological Fluid. *Advances in Materials*, 4, 5. doi: 10.11648/j.am.20150401.11

APPENDICES

A

Sedimentation Experiment Data

| Voltage Reading (V) | | | Period (min) | Voltage Ratio (%) | | |
|---------------------|----------|----------|--------------|-------------------|----------|----------|
| Sample 1 | Sample 2 | Sample 3 | | Sample 1 | Sample 2 | Sample 3 |
| 0 | 0 | 0 | 0 | 0 | 0 | 0 |
| 0 | 0 | 0 | 5 | 0 | 0 | 0 |
| 0 | 0 | 0 | 10 | 0 | 0 | 0 |
| 0 | 0 | 0 | 15 | 0 | 0 | 0 |
| 0 | 0 | 0 | 20 | 0 | 0 | 0 |
| 0 | 0 | 0 | 25 | 0 | 0 | 0 |
| 0 | 0 | 0 | 30 | 0 | 0 | 0 |
| 0 | 0 | 0 | 35 | 0 | 0 | 0 |
| 0 | 0 | 0 | 40 | 0 | 0 | 0 |
| 0 | 0 | 0 | 45 | 0 | 0 | 0 |
| 0 | 0 | 0 | 50 | 0 | 0 | 0 |
| 0 | 0 | 0 | 55 | 0 | 0 | 0 |
| 0 | 0 | 0 | 60 | 0 | 0 | 0 |
| 0.26 | 0 | 0 | 65 | 4.942966 | 0 | 0 |
| 0.68 | 0 | 0 | 70 | 12.92776 | 0 | 0 |
| 1.24 | 0 | 0 | 75 | 23.57414 | 0 | 0 |
| 3.36 | 0 | 0 | 80 | 63.87833 | 0 | 0 |
| 5.26 | 0 | 0 | 85 | 100 | 0 | 0 |
| 5.26 | 0 | 0 | 90 | 100 | 0 | 0 |
| 5.26 | 0 | 0 | 95 | 100 | 0 | 0 |
| 5.26 | 0 | 0 | 100 | 100 | 0 | 0 |
| 5.26 | 0 | 0 | 105 | 100 | 0 | 0 |
| 5.26 | 0 | 0 | 110 | 100 | 0 | 0 |
| 5.26 | 0 | 0 | 115 | 100 | 0 | 0 |
| 5.26 | 0 | 0 | 120 | 100 | 0 | 0 |
| 5.26 | 0 | 0 | 125 | 100 | 0 | 0 |
| 5.26 | 0 | 0 | 130 | 100 | 0 | 0 |
| 5.26 | 0 | 0 | 135 | 100 | 0 | 0 |
| 5.26 | 0 | 0 | 140 | 100 | 0 | 0 |
| 5.26 | 0 | 0 | 145 | 100 | 0 | 0 |

| | | | | | | |
|------|---|------|-----|-----|---|----------|
| 5.26 | 0 | 0 | 150 | 100 | 0 | 0 |
| 5.26 | 0 | 0 | 155 | 100 | 0 | 0 |
| 5.26 | 0 | 0 | 160 | 100 | 0 | 0 |
| 5.26 | 0 | 0 | 165 | 100 | 0 | 0 |
| 5.26 | 0 | 0 | 170 | 100 | 0 | 0 |
| 5.26 | 0 | 0 | 175 | 100 | 0 | 0 |
| 5.26 | 0 | 0 | 180 | 100 | 0 | 0 |
| 5.26 | 0 | 0 | 185 | 100 | 0 | 0 |
| 5.26 | 0 | 0 | 190 | 100 | 0 | 0 |
| 5.26 | 0 | 0 | 195 | 100 | 0 | 0 |
| 5.26 | 0 | 0 | 200 | 100 | 0 | 0 |
| 5.26 | 0 | 0 | 205 | 100 | 0 | 0 |
| 5.26 | 0 | 0 | 210 | 100 | 0 | 0 |
| 5.26 | 0 | 0 | 215 | 100 | 0 | 0 |
| 5.26 | 0 | 0 | 220 | 100 | 0 | 0 |
| 5.26 | 0 | 0 | 225 | 100 | 0 | 0 |
| 5.26 | 0 | 0 | 230 | 100 | 0 | 0 |
| 5.26 | 0 | 0 | 235 | 100 | 0 | 0 |
| 5.26 | 0 | 0 | 240 | 100 | 0 | 0 |
| 5.26 | 0 | 0 | 245 | 100 | 0 | 0 |
| 5.26 | 0 | 0 | 250 | 100 | 0 | 0 |
| 5.26 | 0 | 0 | 255 | 100 | 0 | 0 |
| 5.26 | 0 | 0 | 260 | 100 | 0 | 0 |
| 5.26 | 0 | 0 | 265 | 100 | 0 | 0 |
| 5.26 | 0 | 0 | 270 | 100 | 0 | 0 |
| 5.26 | 0 | 0 | 275 | 100 | 0 | 0 |
| 5.26 | 0 | 0 | 280 | 100 | 0 | 0 |
| 5.26 | 0 | 0 | 285 | 100 | 0 | 0 |
| 5.26 | 0 | 0 | 290 | 100 | 0 | 0 |
| 5.26 | 0 | 0 | 295 | 100 | 0 | 0 |
| 5.26 | 0 | 0 | 300 | 100 | 0 | 0 |
| 5.26 | 0 | 0 | 305 | 100 | 0 | 0 |
| 5.26 | 0 | 0 | 310 | 100 | 0 | 0 |
| 5.26 | 0 | 0 | 315 | 100 | 0 | 0 |
| 5.26 | 0 | 0 | 320 | 100 | 0 | 0 |
| 5.26 | 0 | 0 | 325 | 100 | 0 | 0 |
| 5.26 | 0 | 0 | 330 | 100 | 0 | 0 |
| 5.26 | 0 | 0 | 335 | 100 | 0 | 0 |
| 5.26 | 0 | 0 | 340 | 100 | 0 | 0 |
| 5.26 | 0 | 0 | 345 | 100 | 0 | 0 |
| 5.26 | 0 | 0.01 | 350 | 100 | 0 | 0.190114 |
| 5.26 | 0 | 0 | 355 | 100 | 0 | 0 |
| 5.26 | 0 | 0 | 360 | 100 | 0 | 0 |
| 5.26 | 0 | 0 | 365 | 100 | 0 | 0 |

| | | | | | | |
|------|------|------|-----|-----|----------|----------|
| 5.26 | 0 | 0 | 370 | 100 | 0 | 0 |
| 5.26 | 0 | 0 | 375 | 100 | 0 | 0 |
| 5.26 | 0 | 0 | 380 | 100 | 0 | 0 |
| 5.26 | 0 | 0 | 385 | 100 | 0 | 0 |
| 5.26 | 0 | 0 | 390 | 100 | 0 | 0 |
| 5.26 | 0.02 | 0 | 395 | 100 | 0.380228 | 0 |
| 5.26 | 0.07 | 0 | 400 | 100 | 1.330798 | 0 |
| 5.26 | 0 | 0 | 405 | 100 | 0 | 0 |
| 5.26 | 0.28 | 0 | 410 | 100 | 5.323194 | 0 |
| 5.26 | 0.47 | 0 | 415 | 100 | 8.935361 | 0 |
| 5.26 | 0.68 | 0 | 420 | 100 | 12.92776 | 0 |
| 5.26 | 0.86 | 0 | 425 | 100 | 16.34981 | 0 |
| 5.26 | 1.06 | 0 | 430 | 100 | 20.15209 | 0 |
| 5.26 | 1.28 | 0 | 435 | 100 | 24.3346 | 0 |
| 5.26 | 1.53 | 0 | 440 | 100 | 29.08745 | 0 |
| 5.26 | 1.78 | 0 | 445 | 100 | 33.8403 | 0 |
| 5.26 | 2.04 | 0 | 450 | 100 | 38.78327 | 0 |
| 5.26 | 2.34 | 0 | 455 | 100 | 44.48669 | 0 |
| 5.26 | 2.63 | 0 | 460 | 100 | 50 | 0 |
| 5.26 | 2.89 | 0 | 465 | 100 | 54.94297 | 0 |
| 5.26 | 3.35 | 0 | 470 | 100 | 63.68821 | 0 |
| 5.26 | 3.76 | 0 | 475 | 100 | 71.48289 | 0 |
| 5.26 | 4.14 | 0 | 480 | 100 | 78.70722 | 0 |
| 5.26 | 4.55 | 0 | 485 | 100 | 86.5019 | 0 |
| 5.26 | 4.97 | 0 | 490 | 100 | 94.48669 | 0 |
| 5.26 | 5.26 | 0 | 495 | 100 | 100 | 0 |
| 5.26 | 5.26 | 0 | 500 | 100 | 100 | 0 |
| 5.26 | 5.26 | 0 | 505 | 100 | 100 | 0 |
| 5.26 | 5.26 | 0.02 | 510 | 100 | 100 | 0.380228 |
| 5.26 | 5.26 | 0.04 | 515 | 100 | 100 | 0.760456 |
| 5.26 | 5.26 | 0.07 | 520 | 100 | 100 | 1.330798 |
| 5.26 | 5.26 | 0.11 | 525 | 100 | 100 | 2.091255 |
| 5.26 | 5.26 | 0.14 | 530 | 100 | 100 | 2.661597 |
| 5.26 | 5.26 | 0.13 | 535 | 100 | 100 | 2.471483 |
| 5.26 | 5.26 | 1.47 | 540 | 100 | 100 | 27.94677 |
| 5.26 | 5.26 | 1.95 | 545 | 100 | 100 | 37.07224 |
| 5.26 | 5.26 | 2.15 | 550 | 100 | 100 | 40.87452 |
| 5.26 | 5.26 | 2.57 | 555 | 100 | 100 | 48.85932 |
| 5.26 | 5.26 | 3.01 | 560 | 100 | 100 | 57.22433 |
| 5.26 | 5.26 | 3.57 | 565 | 100 | 100 | 67.87072 |
| 5.26 | 5.26 | 3.9 | 570 | 100 | 100 | 74.14449 |
| 5.26 | 5.26 | 4.33 | 575 | 100 | 100 | 82.31939 |
| 5.26 | 5.26 | 4.51 | 580 | 100 | 100 | 85.74144 |
| 5.26 | 5.26 | 4.69 | 585 | 100 | 100 | 89.1635 |

| | | | | | | |
|------|------|------|-----|-----|-----|----------|
| 5.26 | 5.26 | 5.2 | 590 | 100 | 100 | 98.85932 |
| 5.26 | 5.26 | 5.26 | 595 | 100 | 100 | 100 |
| 5.26 | 5.26 | 5.26 | 600 | 100 | 100 | 100 |
| 5.26 | 5.26 | 5.26 | 605 | 100 | 100 | 100 |
| 5.26 | 5.26 | 5.26 | 610 | 100 | 100 | 100 |
| 5.26 | 5.26 | 5.26 | 615 | 100 | 100 | 100 |
| 5.26 | 5.26 | 5.26 | 620 | 100 | 100 | 100 |
| 5.26 | 5.26 | 5.26 | 625 | 100 | 100 | 100 |
| 5.26 | 5.26 | 5.26 | 630 | 100 | 100 | 100 |
| 5.26 | 5.26 | 5.26 | 635 | 100 | 100 | 100 |
| 5.26 | 5.26 | 5.26 | 640 | 100 | 100 | 100 |
| 5.26 | 5.26 | 5.26 | 645 | 100 | 100 | 100 |
| 5.26 | 5.26 | 5.26 | 650 | 100 | 100 | 100 |
| 5.26 | 5.26 | 5.26 | 655 | 100 | 100 | 100 |
| 5.26 | 5.26 | 5.26 | 660 | 100 | 100 | 100 |
| 5.26 | 5.26 | 5.26 | 665 | 100 | 100 | 100 |
| 5.26 | 5.26 | 5.26 | 670 | 100 | 100 | 100 |
| 5.26 | 5.26 | 5.26 | 675 | 100 | 100 | 100 |
| 5.26 | 5.26 | 5.26 | 680 | 100 | 100 | 100 |
| 5.26 | 5.26 | 5.26 | 685 | 100 | 100 | 100 |
| 5.26 | 5.26 | 5.26 | 690 | 100 | 100 | 100 |
| 5.26 | 5.26 | 5.26 | 695 | 100 | 100 | 100 |
| 5.26 | 5.26 | 5.26 | 700 | 100 | 100 | 100 |
| 5.26 | 5.26 | 5.26 | 705 | 100 | 100 | 100 |
| 5.26 | 5.26 | 5.26 | 710 | 100 | 100 | 100 |
| 5.26 | 5.26 | 5.26 | 715 | 100 | 100 | 100 |
| 5.26 | 5.26 | 5.26 | 720 | 100 | 100 | 100 |
| 5.26 | 5.26 | 5.26 | 725 | 100 | 100 | 100 |
| 5.26 | 5.26 | 5.26 | 730 | 100 | 100 | 100 |
| 5.26 | 5.26 | 5.26 | 735 | 100 | 100 | 100 |
| 5.26 | 5.26 | 5.26 | 740 | 100 | 100 | 100 |
| 5.26 | 5.26 | 5.26 | 745 | 100 | 100 | 100 |
| 5.26 | 5.26 | 5.26 | 750 | 100 | 100 | 100 |
| 5.26 | 5.26 | 5.26 | 755 | 100 | 100 | 100 |
| 5.26 | 5.26 | 5.26 | 760 | 100 | 100 | 100 |
| 5.26 | 5.26 | 5.26 | 765 | 100 | 100 | 100 |
| 5.26 | 5.26 | 5.26 | 770 | 100 | 100 | 100 |
| 5.26 | 5.26 | 5.26 | 775 | 100 | 100 | 100 |
| 5.26 | 5.26 | 5.26 | 780 | 100 | 100 | 100 |
| 5.26 | 5.26 | 5.26 | 785 | 100 | 100 | 100 |
| 5.26 | 5.26 | 5.26 | 790 | 100 | 100 | 100 |
| 5.26 | 5.26 | 5.26 | 795 | 100 | 100 | 100 |
| 5.26 | 5.26 | 5.26 | 800 | 100 | 100 | 100 |
| 5.26 | 5.26 | 5.26 | 805 | 100 | 100 | 100 |

| | | | | | | |
|------|------|------|------|-----|-----|-----|
| 5.26 | 5.26 | 5.26 | 810 | 100 | 100 | 100 |
| 5.26 | 5.26 | 5.26 | 815 | 100 | 100 | 100 |
| 5.26 | 5.26 | 5.26 | 820 | 100 | 100 | 100 |
| 5.26 | 5.26 | 5.26 | 825 | 100 | 100 | 100 |
| 5.26 | 5.26 | 5.26 | 830 | 100 | 100 | 100 |
| 5.26 | 5.26 | 5.26 | 835 | 100 | 100 | 100 |
| 5.26 | 5.26 | 5.26 | 840 | 100 | 100 | 100 |
| 5.26 | 5.26 | 5.26 | 845 | 100 | 100 | 100 |
| 5.26 | 5.26 | 5.26 | 850 | 100 | 100 | 100 |
| 5.26 | 5.26 | 5.26 | 855 | 100 | 100 | 100 |
| 5.26 | 5.26 | 5.26 | 860 | 100 | 100 | 100 |
| 5.26 | 5.26 | 5.26 | 865 | 100 | 100 | 100 |
| 5.26 | 5.26 | 5.26 | 870 | 100 | 100 | 100 |
| 5.26 | 5.26 | 5.26 | 875 | 100 | 100 | 100 |
| 5.26 | 5.26 | 5.26 | 880 | 100 | 100 | 100 |
| 5.26 | 5.26 | 5.26 | 885 | 100 | 100 | 100 |
| 5.26 | 5.26 | 5.26 | 890 | 100 | 100 | 100 |
| 5.26 | 5.26 | 5.26 | 895 | 100 | 100 | 100 |
| 5.26 | 5.26 | 5.26 | 900 | 100 | 100 | 100 |
| 5.26 | 5.26 | 5.26 | 905 | 100 | 100 | 100 |
| 5.26 | 5.26 | 5.26 | 910 | 100 | 100 | 100 |
| 5.26 | 5.26 | 5.26 | 915 | 100 | 100 | 100 |
| 5.26 | 5.26 | 5.26 | 920 | 100 | 100 | 100 |
| 5.26 | 5.26 | 5.26 | 925 | 100 | 100 | 100 |
| 5.26 | 5.26 | 5.26 | 930 | 100 | 100 | 100 |
| 5.26 | 5.26 | 5.26 | 935 | 100 | 100 | 100 |
| 5.26 | 5.26 | 5.26 | 940 | 100 | 100 | 100 |
| 5.26 | 5.26 | 5.26 | 945 | 100 | 100 | 100 |
| 5.26 | 5.26 | 5.26 | 950 | 100 | 100 | 100 |
| 5.26 | 5.26 | 5.26 | 955 | 100 | 100 | 100 |
| 5.26 | 5.26 | 5.26 | 960 | 100 | 100 | 100 |
| 5.26 | 5.26 | 5.26 | 965 | 100 | 100 | 100 |
| 5.26 | 5.26 | 5.26 | 970 | 100 | 100 | 100 |
| 5.26 | 5.26 | 5.26 | 975 | 100 | 100 | 100 |
| 5.26 | 5.26 | 5.26 | 980 | 100 | 100 | 100 |
| 5.26 | 5.26 | 5.26 | 985 | 100 | 100 | 100 |
| 5.26 | 5.26 | 5.26 | 990 | 100 | 100 | 100 |
| 5.26 | 5.26 | 5.26 | 995 | 100 | 100 | 100 |
| 5.26 | 5.26 | 5.26 | 1000 | 100 | 100 | 100 |
| 5.26 | 5.26 | 5.26 | 1005 | 100 | 100 | 100 |
| 5.26 | 5.26 | 5.26 | 1010 | 100 | 100 | 100 |
| 5.26 | 5.26 | 5.26 | 1015 | 100 | 100 | 100 |
| 5.26 | 5.26 | 5.26 | 1020 | 100 | 100 | 100 |
| 5.26 | 5.26 | 5.26 | 1025 | 100 | 100 | 100 |

| | | | | | | |
|------|------|------|------|-----|-----|-----|
| 5.26 | 5.26 | 5.26 | 1030 | 100 | 100 | 100 |
| 5.26 | 5.26 | 5.26 | 1035 | 100 | 100 | 100 |
| 5.26 | 5.26 | 5.26 | 1040 | 100 | 100 | 100 |
| 5.26 | 5.26 | 5.26 | 1045 | 100 | 100 | 100 |
| 5.26 | 5.26 | 5.26 | 1050 | 100 | 100 | 100 |
| 5.26 | 5.26 | 5.26 | 1055 | 100 | 100 | 100 |
| 5.26 | 5.26 | 5.26 | 1060 | 100 | 100 | 100 |
| 5.26 | 5.26 | 5.26 | 1065 | 100 | 100 | 100 |
| 5.26 | 5.26 | 5.26 | 1070 | 100 | 100 | 100 |
| 5.26 | 5.26 | 5.26 | 1075 | 100 | 100 | 100 |
| 5.26 | 5.26 | 5.26 | 1080 | 100 | 100 | 100 |
| 5.26 | 5.26 | 5.26 | 1085 | 100 | 100 | 100 |
| 5.26 | 5.26 | 5.26 | 1090 | 100 | 100 | 100 |
| 5.26 | 5.26 | 5.26 | 1095 | 100 | 100 | 100 |
| 5.26 | 5.26 | 5.26 | 1100 | 100 | 100 | 100 |
| 5.26 | 5.26 | 5.26 | 1105 | 100 | 100 | 100 |
| 5.26 | 5.26 | 5.26 | 1110 | 100 | 100 | 100 |
| 5.26 | 5.26 | 5.26 | 1115 | 100 | 100 | 100 |
| 5.26 | 5.26 | 5.26 | 1120 | 100 | 100 | 100 |
| 5.26 | 5.26 | 5.26 | 1125 | 100 | 100 | 100 |
| 5.26 | 5.26 | 5.26 | 1130 | 100 | 100 | 100 |
| 5.26 | 5.26 | 5.26 | 1135 | 100 | 100 | 100 |
| 5.26 | 5.26 | 5.26 | 1140 | 100 | 100 | 100 |
| 5.26 | 5.26 | 5.26 | 1145 | 100 | 100 | 100 |
| 5.26 | 5.26 | 5.26 | 1150 | 100 | 100 | 100 |
| 5.26 | 5.26 | 5.26 | 1155 | 100 | 100 | 100 |
| 5.26 | 5.26 | 5.26 | 1160 | 100 | 100 | 100 |
| 5.26 | 5.26 | 5.26 | 1165 | 100 | 100 | 100 |
| 5.26 | 5.26 | 5.26 | 1170 | 100 | 100 | 100 |
| 5.26 | 5.26 | 5.26 | 1175 | 100 | 100 | 100 |
| 5.26 | 5.26 | 5.26 | 1180 | 100 | 100 | 100 |
| 5.26 | 5.26 | 5.26 | 1185 | 100 | 100 | 100 |
| 5.26 | 5.26 | 5.26 | 1190 | 100 | 100 | 100 |
| 5.26 | 5.26 | 5.26 | 1195 | 100 | 100 | 100 |
| 5.26 | 5.26 | 5.26 | 1200 | 100 | 100 | 100 |
| 5.26 | 5.26 | 5.26 | 1205 | 100 | 100 | 100 |
| 5.26 | 5.26 | 5.26 | 1210 | 100 | 100 | 100 |
| 5.26 | 5.26 | 5.26 | 1215 | 100 | 100 | 100 |
| 5.26 | 5.26 | 5.26 | 1220 | 100 | 100 | 100 |
| 5.26 | 5.26 | 5.26 | 1225 | 100 | 100 | 100 |
| 5.26 | 5.26 | 5.26 | 1230 | 100 | 100 | 100 |
| 5.26 | 5.26 | 5.26 | 1235 | 100 | 100 | 100 |
| 5.26 | 5.26 | 5.26 | 1240 | 100 | 100 | 100 |
| 5.26 | 5.26 | 5.26 | 1245 | 100 | 100 | 100 |

| | | | | | | |
|------|------|------|------|-----|-----|-----|
| 5.26 | 5.26 | 5.26 | 1250 | 100 | 100 | 100 |
| 5.26 | 5.26 | 5.26 | 1255 | 100 | 100 | 100 |
| 5.26 | 5.26 | 5.26 | 1260 | 100 | 100 | 100 |
| 5.26 | 5.26 | 5.26 | 1265 | 100 | 100 | 100 |
| 5.26 | 5.26 | 5.26 | 1270 | 100 | 100 | 100 |
| 5.26 | 5.26 | 5.26 | 1275 | 100 | 100 | 100 |
| 5.26 | 5.26 | 5.26 | 1280 | 100 | 100 | 100 |
| 5.26 | 5.26 | 5.26 | 1285 | 100 | 100 | 100 |
| 5.26 | 5.26 | 5.26 | 1290 | 100 | 100 | 100 |
| 5.26 | 5.26 | 5.26 | 1295 | 100 | 100 | 100 |
| 5.26 | 5.26 | 5.26 | 1300 | 100 | 100 | 100 |
| 5.26 | 5.26 | 5.26 | 1305 | 100 | 100 | 100 |
| 5.26 | 5.26 | 5.26 | 1310 | 100 | 100 | 100 |
| 5.26 | 5.26 | 5.26 | 1315 | 100 | 100 | 100 |
| 5.26 | 5.26 | 5.26 | 1320 | 100 | 100 | 100 |
| 5.26 | 5.26 | 5.26 | 1325 | 100 | 100 | 100 |
| 5.26 | 5.26 | 5.26 | 1330 | 100 | 100 | 100 |
| 5.26 | 5.26 | 5.26 | 1335 | 100 | 100 | 100 |
| 5.26 | 5.26 | 5.26 | 1340 | 100 | 100 | 100 |
| 5.26 | 5.26 | 5.26 | 1345 | 100 | 100 | 100 |
| 5.26 | 5.26 | 5.26 | 1350 | 100 | 100 | 100 |
| 5.26 | 5.26 | 5.26 | 1355 | 100 | 100 | 100 |
| 5.26 | 5.26 | 5.26 | 1360 | 100 | 100 | 100 |
| 5.26 | 5.26 | 5.26 | 1365 | 100 | 100 | 100 |
| 5.26 | 5.26 | 5.26 | 1370 | 100 | 100 | 100 |
| 5.26 | 5.26 | 5.26 | 1375 | 100 | 100 | 100 |
| 5.26 | 5.26 | 5.26 | 1380 | 100 | 100 | 100 |
| 5.26 | 5.26 | 5.26 | 1385 | 100 | 100 | 100 |
| 5.26 | 5.26 | 5.26 | 1390 | 100 | 100 | 100 |
| 5.26 | 5.26 | 5.26 | 1395 | 100 | 100 | 100 |
| 5.26 | 5.26 | 5.26 | 1400 | 100 | 100 | 100 |
| 5.26 | 5.26 | 5.26 | 1405 | 100 | 100 | 100 |
| 5.26 | 5.26 | 5.26 | 1410 | 100 | 100 | 100 |
| 5.26 | 5.26 | 5.26 | 1415 | 100 | 100 | 100 |
| 5.26 | 5.26 | 5.26 | 1420 | 100 | 100 | 100 |
| 5.26 | 5.26 | 5.26 | 1425 | 100 | 100 | 100 |
| 5.26 | 5.26 | 5.26 | 1430 | 100 | 100 | 100 |
| 5.26 | 5.26 | 5.26 | 1435 | 100 | 100 | 100 |
| 5.26 | 5.26 | 5.26 | 1440 | 100 | 100 | 100 |